FISEVIER

Contents lists available at ScienceDirect

Palaeogeography, Palaeoclimatology, Palaeoecology

journal homepage: www.elsevier.com/locate/palaeo



Biosediment assemblages reveal disrupted silica cycling and redox conditions throughout the Rhaetian Stage: Evidence for a precursor event to the end-Triassic mass extinction

Annaka M. Clement ^{a,1,*}, Lydia S. Tackett ^{b,1}, Samuel Marolt ^c

- ^a Denver Museum of Nature and Science, 2001 Colorado Blvd., Denver, CO 80205, USA
- ^b University of Missouri, Department of Geological Sciences, Columbia, MO 65201, USA
- ^c North Dakota State University, Department of Earth, Environmental, and Geospatial Sciences, Fargo, ND 58108, USA

ARTICLEINFO

Editor: L Angiolini

Keywords:
Norian-Rhaetian boundary
Late Triassic
Microfossils
Sponges
Volcanism
Redox proxies
End-Triassic mass extinction

ABSTRACT

The Norian-Rhaetian boundary (Late Triassic) represents an important precursor extinction event to the end-Triassic mass extinction, but the biotic and geochemical shifts are not well-understood due to poor stratigraphic constraints. Here we examine the microfossil record for metazoans and protists on a Panthalassan carbonate ramp (Gabbs Formation, Nevada, U.S.A.) during the late Norian to mid-Rhaetian, and correlate changes in these assemblages with macrofossil shifts and geochemical data (strontium and carbon isotopes). In the latest Norian, demosponge spicules represent a small proportion of shallow marine biosediments. Demosponges are joined in the earliest Rhaetian by increasingly abundant hypersilicified sponge spicules and silica-limited hexactinellid sponge spicules synchronous with a negative strontium isotope excursion indicating increased hydrothermal or volcanic activity. Common carbonate microfossils such as echinoderm ossicles and ostracods are typically silicified in these deposits as well, suggesting increased silicic porewater. The source for increased dissolved silica in shallow marine systems is suggested to be hydrothermal vent degassing, likely associated with increased tectonic rifting activity. Mid-Rhaetian microfossil assemblages exhibit evidence for intermitted anoxia in reducing conditions, supporting a scenario in which environmental stress was a prolonged feature of much of the Rhaetian Stage, rather than a short-term event in the terminal Rhaetian. While there is no marine sedimentary record of volcanism recognized for this interval, biosedimentary assemblages may serve as proxies for geochemical conditions associated with rifting.

1. Introduction

The Late Triassic is an interval of significant environmental change. Recent work has recognized that much of this change may have taken place in the latest Norian and earliest Rhaetian (Callegaro et al., 2012; Zaffani et al., 2017, 2018; Rigo et al., 2020; Schoepfer et al., 2022). The Norian–Rhaetian boundary (NRB) is not well understood, however, and exploration of the potential geochemical shifts near the boundary and the implications for the environmental upheaval at the end of the Triassic Period are only beginning. Additionally, faunal turnover at the NRB is poorly constrained, as many Norian–Rhaetian or Upper Triassic sections are undifferentiated, but a decline in the biodiversity of ammonoids, bivalves, and conodonts as well as a major turnover in

radiolarians across the NRB (Lucas and Tanner, 2018; Rigo et al., 2020) suggests that an end-Norian extinction event may have occurred, the causes of which are not presently known (Rigo et al., 2020). With numerous remaining unknowns, the Late Triassic, and NRB specifically, present a promising opportunity to evaluate the environmental, geochemical, and faunal changes leading into a mass extinction.

Multiple stable isotope systems support the hypothesis that the earliest Rhaetian was a time of significant geochemical shifts. Beginning with an apparently global organic carbon isotope excursion (CIE) in marine deposits across the NRB (Zaffani et al., 2017; Rigo et al., 2020), the early Rhaetian is also associated with faunal turnover in both macrofossils (Laws, 1982; Tackett and Bottjer, 2016) and microfossils, including radiolarians and conodonts (see Rigo et al., 2020).

^{*} Corresponding author at: Denver Museum of Nature and Science, 2001 Colorado Blvd., Denver, CO 80205, USA *E-mail address*: annaka.clement@dmns.org (A.M. Clement).

¹ Indicates co-first authors.

Additionally, a substantial negative strontium isotope excursion (SIE) begins at the NRB and continues to fall until the Middle Jurassic (Korte et al., 2003; Callegaro et al., 2012; Tackett et al., 2014; Kovács et al., 2020). Strontium isotopic values reflect the relative input of eroded continental crust (more positive values) or eroded basalts, hydrothermal fluids, or volcanic degassing inputs (more negative values) (Taylor and Lasaga, 1999; Veizer et al., 1999). The negative SIE in the Early Jurassic has been previously interpreted to reflect the non-radiogenic input of weathered of basalts associated with the emplacement of the Central Atlantic Magmatic Province (CAMP) (Tackett et al., 2014; Korte et al., 2019), though this excursion begins at the NRB, suggesting an earlier geochemical influx of non-radiogenic strontium. The potential sources for the SIE (increased rifting rates, volcanic activity, rapid ophiolitic erosion) could also be expected to cause environmental changes. The latest Rhaetian is also marked by a significant negative CIE associated with the end-Triassic mass extinction interval and acidifying conditions in the oceans (Guex et al., 2004; Ward et al., 2007; Guex et al., 2009; Greene et al., 2012; Thibodeau et al., 2016; Korte et al., 2019). A precursor negative CIE found below the extinction interval in the Gabbs Formation of western Nevada, USA, (Larina et al., 2021) provides additional evidence that the Rhaetian experienced multiple geochemical and possibly environmental shifts throughout its duration.

The implementation of a microfossil survey, which includes all taxonomic groups and their preservation, provides useful insights to environmental and faunal changes that are not well expressed in the rock or macrofossil records. Biogenic sediments of many kinds make up a considerable amount of the carbonate rocks which record the NRB through the end of the Triassic in North America, and most microfossil studies focus on the dynamics of one or two specific groups (e.g., radiolarians and conodonts). Biosediments not only provide important faunal information, they may also be used as proxies for specific environmental features. For example, the proliferation of lithistid demosponge spicules in the Lower Jurassic deposits from the Sunrise Formation are interpreted to represent evidence for increased dissolved silica (silicic acid or DSi) as a result of volcanic erosion related to CAMP volcanism (Ritterbush et al., 2014, 2016). Accumulations of phosphatic microfossils, like teeth, have been used as evidence of condensation to recognize important sequence stratigraphic surfaces such as transgressive surfaces and maximum flooding surfaces (Kidwell, 1989; Föllmi, 2016).

Changes in the taphonomy of microfossils may also indicate changes in pore water geochemistry. The phosphatization of microfossils can be linked with early diagenesis resulting from altered pore water redox conditions (Brett and Baird, 1986; Dattilo et al., 2019; Freeman et al., 2019). Likewise, the pyritization of fossils is often associated with lowered oxygen and pH in pore waters (Brett and Baird, 1986). Conversely, early silicification of fossils in shallow sediments necessitates only a slight decrease in pH (enough to preference silica deposition over carbonate) and silica-saturated pore waters. While the preservation of microfossils can be informative as individual groups (original mineralogy, silicified, pyritized, and phosphatized), together they can provide a suite of proxy data that illustrate geochemical changes in the shallow marine sediments, many of which (dysoxia and acidification most notably) impacted the benthic community as a whole.

Furthermore, biogenic sediments can also reveal population dynamics of taxa that are unlikely to preserve as articulated specimens, such as vertebrates, echinoderms, and sponges. Whole sponges are not commonly found in macrofossil studies and have largely gone unreported as a component of the benthic community in the Gabbs Formation (Laws, 1978, 1982; Tackett and Bottjer, 2016). Sponge spicules can also be difficult to discern in petrographic thin section analysis due to rarity or surrounding silicification. Many paleoecological analyses depend on shelly invertebrate macrofossils to characterize ecological structure and faunal change but are likely to overlook many-element taxa despite their prolific biogenic mineral production. Thus, microfossils can provide important information about the presence and

abundance of macrofauna in shallow marine environments.

The Gabbs Formation in Nevada, U.S.A., represents an ideal stratigraphic interval to document biosediment populations and preservation given its extensive biostratigraphic (Laws, 1982; Orchard et al., 2007; Taylor et al., 2021), and sedimentological frameworks (Taylor et al., 1983; Clement and Tackett, 2021), paleoecological work (Muller and Ferguson, 1936, 1939; Laws, 1982; Tackett and Bottjer, 2016), and developing Norian-Rhaetian geochemical framework (Rigo et al., 2020). In this interval, macrofossil benthic assemblages, composed of primarily shelly invertebrates, show both faunal and ecological turnover; however, few studies have documented changes in multi-element invertebrates or their vertebrate predators more often preserved as microfossils. Microfossil assemblages and their preservation may also shed light on geochemical changes across the NRB indicated by recent carbon isotopic evidence (Rigo et al., 2020) and correlative strontium isotope excursions (Veizer et al., 1999; Korte et al., 2003; Tackett et al., 2014). The sedimentological framework of the Gabbs Formation also aids in studies across the NRB in addition to containing a well-studied Triassic-Jurassic boundary (TJB) section adding useful long-term geologic context (Laws, 1982; Taylor et al., 1983; Hallam and Wignall, 2000; Guex et al., 2004; Clement and Tackett, 2021). Recent sedimentological work in the Rhaetian provided evidence that in the latest Triassic, ocean acidification was decoupled from the loss of carbonate facies in the Gabbs Formation (Clement and Tackett, 2021). However, detailed correlation of geochemical, biological, and sedimentological changes is poorly constrained below the end-Triassic mass extinction interval, despite evidence for significant changes in seafloor spreading (Callegaro et al., 2012; Kovács et al., 2020) and faunal change in the latest Norian and across the NRB (Tackett et al., 2014; Tackett and Bottjer, 2016). The sedimentological, geochemical, and biological frameworks present in the Gabbs Formation allow for a facies-controlled survey of microfossil assemblages from the late Norian to the mid-Rhaetian to better define environmental and faunal shifts in eastern Panthalassa and place them in a regional and global context.

1.1. Geologic setting

The Gabbs Formation, in its type-area in the vicinity of New York Canyon (Fig. 1), is divided into three members; the Nun Mine Member, Mount Hyatt Member, and the Muller Canyon Member (Taylor et al., 1983). These members, both the older informal units and present members, were originally defined on lithology (Muller and Ferguson, 1936, 1939; Taylor et al., 1983) with the Nun Mine Member consisting primarily of shales with minor lime mudstone, the Mount Hyatt Member consisting of primarily grainy carbonate beds (mudstone-packstone and floatstone beds), and the Muller Canyon Member consisting of siltstone with carbonate cement (Muller and Ferguson, 1936, 1939; Laws, 1982; Taylor et al., 1983; Clement and Tackett, 2021). The facies that comprise these members were further defined by Clement and Tackett (2021). With this stratigraphic framework, the Nun Mine Member primarily consists of interbedded calcareous shale (facies CS) and purple lime mudstone (facies PLM), the lower part of Mount Hyatt member of shallowing-upwards packages of skeletal packstone-floatstone (facies SPF) and hashy skeletal packstone (facies HSP), the upper part of the Mount Hyatt Member of interbedded silty lime mudstone-wackestone (facies SLMW) and calcareous siltstone (facies CSt) (Clement and Tackett, 2021). Together these are interpreted to represent a shallowingupwards mixed carbonate-siliciclastic ramp.

The Gabbs Formation also contains two important boundaries, the Norian–Rhaetian boundary (NRB) and the Triassic–Jurassic boundary (TJB). The NRB is classically defined by ammonoid and conodont biostratigraphy (Taylor and Guex, 2002; Orchard et al., 2007; Taylor et al., 2021) and has historically been placed within or below the Nun Mine Member biostratigraphically, based on the ranges of the ammonoid *Paracochloceras amoenum* Mojsisovics, 1893 (Taylor and Guex, 2002; Taylor et al., 2021) and conodonts *Epigondolella mosheri* (Kozur

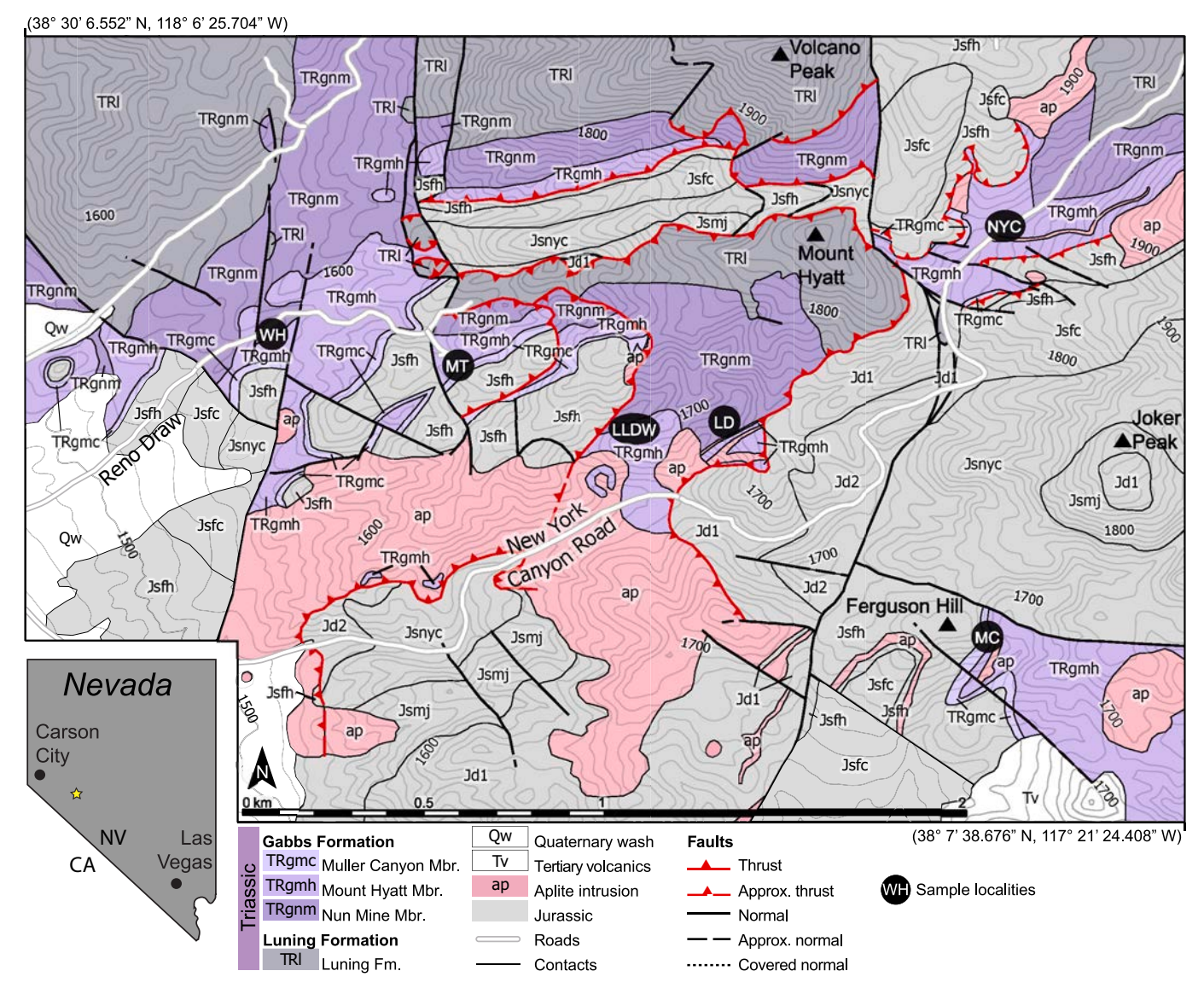


Fig. 1. Regional and geological map of New York Canyon in the Gabbs Valley Range, Nevada, U.S.A. The geological map is modified from Clement and Tackett (2021) to depict the Late Triassic localities in the New York Canyon area that were sampled for microfossils. Locality names: WH- Windy Hill, MT- Mine Test, LLDW-Lower Luning Draw West, LD- Luning Draw, NYC- New York Canyon Road, MC- Muller Canyon. Map area: northwest corner (38° 30′ 6.552" N, 118° 6′ 25.704" W), southeast corner (38° 7′ 38.676" N, 117° 21′ 24.408" W). GPS locations of the individual measured sections are available in Supplemental Table 1.

and Mostler, 1971) Buryi, 1989 and Epigondolella bidentata Mosher, 1968 (Orchard et al., 2007). Strontium isotope analysis by Tackett et al. (2014) showed the ⁸⁷Sr/⁸⁶Sr shift from higher and more erratic Norian values in the lower portion of the Mount Hyatt Member [identified in Tackett et al., 2014 as the Nun Mine Member] to lower and more stable Rhaetian values in the upper portion of the Mount Hyatt Member, thus placing the NRB higher in the stratigraphy within the Mount Hyatt Member. A negative carbon isotope perturbation at approximately the same stratigraphic position as the strontium shift, supports this slightly higher position of the NRB (Rigo et al., 2020). Though these positions of the NRB may appear in conflict, the strontium and carbon isotope shifts are observed in a portion of the section not typically sampled for biostratigraphy owing to a low abundance of ammonite fossils and few shaly units. The lack of biostratigraphy data from this portion of the section may account for the discrepancy in boundary location [though see Lei et al., 2022's discussion on the possible early Rhaetian placement of the ⁸⁷Sr/⁸⁶Sr excursion]. The TJB is found within the Muller Canyon Member and is indicated by the first appearance of Jurassic ammonite Psiloceras spelae Guex et al., 1998 (Taylor and Guex, 2002; Guex et al., 2004; Ward et al., 2007; Taylor et al., 2021).

This work utilizes material collected from six localities of the Gabbs Formation with stratigraphic sections measured in Clement and Tackett (2021); Windy Hill (WH), Mine Test (MT), Lower Lunding Draw West (LLDW), Luning Draw Type Section (LD), New York Canyon Road (NYC), and Muller Canyon (MC) (Supplemental Fig. 1). Samples from the uppermost 10 m of the Nun Mine Member were collected from the Windy Hill, Luning Draw Type Section, and New York Canyon Road localities. Samples from the approximately 50 m of the Mount Hyatt Member were collected from the Windy Hill, Mine Test, Lower Luning Draw West, New York Canyon Road, and Muller Canyon localities.

2. Methods

Samples were collected from six of the eight stratigraphic sections measured in Clement and Tackett (2021), totaling 41 samples examined for microfossils. Most samples (26) were selected from existing lithologic and bulk macrofossil samples of the skeletal packstone–floatstone facies in Mount Hyatt Member (middle member) of the Gabbs Formation owing to its larger overlap among columns (Clement and Tackett, 2021) (Supplemental Fig. 1), its previous study for macrofossils (Muller and

Ferguson, 1936; Laws, 1978, 1982; Hallam and Wignall, 2000; Tackett and Bottjer, 2016; Larina et al., 2021; Taylor et al., 2021), the chemostratigraphic position if the Norian–Rhaetian boundary (NRB) within this unit (Tackett et al., 2014; though see Lei et al. (2022) for other placement), and stable isotope characterization of the section (Rigo et al., 2020). For comparison among facies, 7 samples were selected from the purple lime mudstone (PLM) and 8 from the silty lime mudstone–wackestone facies (SLMW) (Clement and Tackett, 2021).

For each sample, carbonate lithology, following the modified Dunham Classification system (Dunham, 1962; Embry and Klovan, 1971), and facies interpretations, according to Clement and Tackett (2021), were made using thin section petrography, bedding characteristics, sedimentary structures, contacts, and macrofossils. Carbonate material from these samples was further analyzed for microfossil material including ichthyoliths. Following the buffered acetic acid solution method outlined in Jeppsson et al. (1999), approximately 5-30 g of rock fragments were placed in fiberglass net baskets and submerged in buffered acetic acid solution. Buffered solutions were produced by submerging rock fragments in 10% Glacial acetic acid for at least 24 h or until there was no reaction with the solution. The resulting solution, now containing dissolved carbonate, was then mixed with 12 M Glacial acetic acid and deionized water at a ratio of 30:7:63. A subset of sediment residues was produced using an unbuffered 10% acetic acid solution. Sediment residues were then sieved into size fractions (>250 µm, $125-250 \mu m$, $75-125 \mu m$, and $< 75 \mu m$).

The $>\!250~\mu m$ size fraction was analyzed under a Zeiss V.12 Focus Precision microscope, and microfossils and relevant abiogenic sediments were attached to gridded microfossil trays using gum Arabic. In order to establish abundance and higher-order diversity of microfossil assemblages, the first 100 identifiable microfossils encountered (excluding coprolites) were used for the analysis. Microfossils were identified to the phylum or class taxonomic level, and rarefactions were generated from these categories to confirm adequate sampling (Supplemental Fig. 2). Additional notes on each microfossil were made regarding taphonomy, preservation mineralogy, and quality. Samples containing less than five microfossils in the first 5 cm³ of material picked were removed from the analysis. Of the original 41 samples selected and processed, 34 samples produced microfossils and were used in the analysis (24 facies SPF, 4 facies PLM, 6 facies SLMW).

2.1. SEM and EDS analysis

A limited number of extracted microfossils representing major taxonomic groups and modes of preservation were selected for photography and energy-dispersive spectroscopy (EDS) using a scanning electron microscope (SEM). Specimens were adhered to a modified paper tray using gum Arabic. Sample trays were attached to cylindrical aluminum mounts with carbon adhesive tape (Ted Pella, Redding, California, USA). Mounted specimens were sputter coated (Cressington 108auto, Ted Pella, Redding, California, USA) with a conductive layer of gold. Images were obtained with a JEOL JSM-6490LV scanning electron microscope (JEOL USA, Inc., Peabody MA, USA); energy-dispersive X-ray information was collected at an accelerating voltage of 15 kV using a Thermo Scientific UltraDry silicon drift detector and Noran System Seven imaging system (ThermoFisher Scientific, Madison WI, USA).

2.2. Quantitative analysis

Quantitative analysis of microfossil samples was carried out in R (R Core Team, 2022) using RStudio (RStudio Team, 2022). Diversity was calculated for each facies through time at the lowest taxonomic classifications possible. Both Shannon's H and Simpson's 1-D diversity metrics were used to account for the impact of hyper-abundant taxa. Evenness was calculated using Pielou's J derived from the Shannon's H calculations. Diversity and evenness metrics were calculated using the R package Vegan (Oksanen et al., 2022) in conjunction with the package

Boot (Canty and Ripley, 2021; Davison and Hinkley, 1997) to generate confidence intervals using the bootstrapping method with 1000 iterations. Cluster analysis and non-metric multidimensional scaling ordination (NMDS) was carried out to identify broad trends in the data using the R packages Cluster and Vegan (Maechler et al., 2021; Oksanen et al., 2022). Co-occurrence of microfossils (based on presence/absence) with one another and within specific facies and measured sections was analyzed in a pairwise fashion using the R package Cooccur (Griffith et al., 2016). Co-occurrence analysis was run both with and without singleton taxa to identify and reduce their impact on overall trends. Co-occurrence analyses were also run on microfossil grouping based on preservation style, referred to herein as "taphotaxa". Additional comparisons of specific microfossil taxa were carried out using xy plots.

3. Results

3.1. Taxonomic diversity

Sample residues produced microfossils from nine phyla; Foraminifera, Retaria (radiolarians), Porifera, Mollusca (bivalves, gastropods, cephalopods), Bryozoa, Brachiopoda, Arthropoda (ostracods), Echinodermata, and Chordata (Table 1, Fig. 2). Shannon's H and Simpson's 1-D indices decline across the Norian–Rhaetian boundary (NRB) within facies SPF (Fig. 3). Evenness was low among all facies but increases in the NRB interval, attributable to an increase in siliceous sponge spicules (from both hexactinellid sponges and lithistid demosponges), which were not previously observed in facies SPF. Diversity in facies SPF and SLMW remained similar in the Rhaetian samples though tended to be lower than the diversity in facies SPF from the latest Norian (Fig. 3).

3.2. Cluster and NMDS analysis

Cluster and non-metric multidimensional scaling ordination (NMDS) analyses based on the liberated microfossil assemblages were applied to the entire microfossil dataset to aid in the identification of temporal and facies trends. Cluster analysis of microfossil assemblages categorized at the highest useful taxonomic level (phylum, sub-phylum, class, or order) to reflected similarities in dominant microfossil components in a given sample and did not cluster based on relative age or facies (Fig. 4A). Microfossil assemblages from New York Canyon Road always exhibited higher similarity to each other than to samples from other sections, except when sponge spicules were the dominant group, in which case they clustered with other sponge-dominated assemblages from other stratigraphic sections (e.g., Windy Hill, Luning Draw) (Fig. 4A).

NMDS analysis on the microfossil assemblages agreed with the cluster analysis in that resultant groups were primarily determined by the high abundance of a microfossil taxon in a given sample (Fig. 4A, B). Axis 1 of the NMDS analysis appeared to be determined by the presence of hyper-abundant microfossil taxa dominating the sample (e.g., echinoderm stereom, hexactinellid spicules, or lithistid demosponge spicules) all of which occurred frequently in New York Canyon Road samples and only rarely in other measured sections, regardless of facies. For this reason, when analyzing specific trends in microfossils, New York Canyon Road was often considered separately from other samples.

3.3. Co-occurrence analysis

Co-occurrence analysis on the entire dataset using taphotaxa microfossil groups was run both including and excluding singleton taphotaxa occurrences (Fig. 5A). In both cases vertebrate microfossils (teeth, denticles, scales, and bone fragments) tended to co-occur. The inclusion of singletons extended this co-occurrence to gastropod and bivalve internal molds and echinoderm spines, which share a similar phosphatized mineralogy. Taphotaxa co-occurrence, both with and without singletons, also demonstrated that lithistid demosponge spicules tended not to be found with vertebrate material (teeth and bone

NYC66.6b

NYC66.6

NYC72.2

Table 1
Microfossil assemblages identified by taxonomic group and taphonomy.

MC8

MC5.9

MT19.9

MT17.5

MT2.15

NYC87.6

								111 000100	
Facies	SLMW	SLMW	SLMW	SLMW	SLMW	SLMW	SPF	SPF	SPF
Age	Rhaetian	Rhaetian	Rhaetian	Rhaetian	Rhaetian	Rhaetian	Rhaetian	Rhaetian	Rhaetian
Foraminifera	0	1	0	0	0	0	0	0	0
Radiolarian	0	0	0	0	0	0	0	0	0
Sphinctozoan sponge	0	0	0	0	0	0	0	0	0
Non-lithistid demosponge spicule	1	1	4	0	21	0	0	3	9
Lithistid demosponge spicule	0	0	9	0	0	93	52	5	10
Hexactinellid spicule	4	0	7	3	0	7	29	6	29
Bryozoan	0	0	0	0	0	0	0	0	0
Brachiopod	0	0	0	0	0	0	0	0	0
Gastropod	0 0	0 1	0	0	0 0	0	0	0 0	0 4
Gastropod internal mold Bivalve	0	4	0	1	0	0	0	0	0
Bivalve fragment	25	8	15	19	1	0	0	4	2
Bivalve internal mold	0	14	0	0	0	0	0	0	0
Cephalopod hooklet	0	0	0	0	0	0	0	0	0
Ammonoid	0	0	0	0	0	0	0	0	0
Ostracod	0	0	37	43	75	0	0	31	3
Echinoderm spine	1	12	2	4	0	0	0	3	7
Echinoderm stereom	4	0	0	0	2	0	18	39	36
Conodont	0	0	0	0	0	0	0	0	0
Denticle	0	6	2	0	0	0	0	0	0
Scale	0	0	0	4	0	0	0	0	0
Scale fragment	39	0	15	11	0	0	1	1	0
Bone fragment	21	5	9	11	1	0	0	3	0
Tooth	5	48	0	4	0	0	0	5	0
Jaw palate fragment	0	0	0	0	0	0	0	0	0
Total microfossils Richness	100 8	100 10	100 9	100 9	100 5	100 2	100 4	100 10	100 8
ricinicss	O	10	,	,	3	2	7	10	O
	WH32.65	WH32.4	WH26.9	WH26.35	WH16.7	WH6.5	WH2	NYC65.4	NYC62
Facies	SPF	SPF	SPF	SPF	SPF	PLM	PLM	SPF	SPF
Age	NRB	NRB	Norian	Norian	Norian	Norian	Norian	Rhaetian	NRB
Foraminifera	0	0	0	22	0	0	0	0	0
Radiolarian	0	0	0	0	0	0	0	0	0
Sphinctozoan sponge	0	0	0	0	0	0	0	0	3
Non-lithistid demosponge spicule	3	3	4	1	1	87	24	4	6
Lithistid demosponge spicule	82	9	42	0	0	0	0	35	1
Hexactinellid spicule	0	0	0	0	0	0	0	2	15
Bryozoan	0	0 0	0	0	0	0	0	0 0	0
Brachiopod Gastropod	0	1	0	0	1	0	0	0	0
Gastropod internal mold	1	24	12	13	21	1	0	0	0
Bivalve	0	0	0	0	0	0	0	0	0
Bivalve fragment	6	11	9	31	7	0	0	0	1
Bivalve internal mold	0	0	0	0	0	0	0	0	0
Cephalopod hooklet	0	0	0	0	0	0	0	0	0
Ammonoid	0	0	0	0	0	0	0	0	0
Ostracod	0	15	6	3	0	1	0	3	2
Echinoderm spine	4	17	4	16	3	2	2	2	6
Echinoderm stereom	0	12	12	3	56	0	0	52	66
Conodont	0	0	0	0	0	0	0	0	0
Denticle	0	1	0	0	4	2	0	0	0
Scale	0	0	0	1	0	0	0	0	0
Scale fragment	2	3	8	4	1	1	9	0	0
Bone fragment	2	1	1	2	0	4	9	0	0
Tooth	0	3	2	4	6	2	53	2	0
Jaw palate fragment Total microfossils	0	0	0	0	0	0	3	0	0
Richness	100 7	100 12	100 10	100 11	100 9	100 8	100 6	100 7	100 8
riciniess	,	12	10	11	9	0	O	,	0
	, marcon .	\mu=1			,,,,,,,,,,,,,,,,,,,,,,,,,,,,,,,,,,,,,,,		,		
	NYC61.1	NYC58.5b	NYC58.5	NYC54	NYC51.4	NYC46	NYC43.6	NYC40.5	NYC40
Facies	SPF	SPF	SPF	SPF	SPF	SPF	SPF	SPF	SPF
Age	NRB	NRB	NRB	Norian	Norian	Norian	Norian	Norian	Norian
Foraminifera	0	0	3	1	0	1	2	0	0
Radiolarian	0	0	0	0	0	0	0	0	0
		_	_	_	_	_		_	_
Sphinctozoan sponge	0	0	0	0	0	0	0	0	0

5

Table 1 (continued)

Facies Age	NYC61.1	NYC58.5b SPF NRB	NYC58.5 SPF NRB	NYC54 SPF Norian	NYC51.4 SPF Norian	NYC46 SPF Norian	NYC43.6 SPF Norian	NYC40.5 SPF Norian	SPF Norian
	SPF NRB								
Lithistid demosponge spicule	3	3	4	0	0	0	3	18	94
Hexactinellid spicule	0	0	1	0	0	3	3	0	0
Bryozoan	0	0	0	0	0	0	0	0	0
Brachiopod	0	0	0	0	0	0	0	0	0
Gastropod	0	0	0	1	0	0	0	0	0
Gastropod internal mold	0	0	0	13	19	15	1	8	0
Bivalve	0	0	0	1	0	1	0	0	0
Bivalve fragment	0	2	0	1	2	5	5	0	0
Bivalve internal mold	0	0	0	0	0	2	0	0	0
Cephalopod hooklet	0	0	0	0	0	0	0	0	0
Ammonoid	0	0	0	0	0	0	0	0	0
Ostracod	1	5	0	2	9	17	23	0	0
Echinoderm spine	2	0	14	8	18	3	3	6	0
Echinoderm stereom	89	87	77	71	41	41	53	62	6
Conodont	0	0	0	0	0	0	0	0	0
Denticle	0	0	0	0	1	0	0	0	0
Scale	0	0	0	0	0	0	0	0	0
Scale fragment	0	0	0	0	3	1	0	0	0
Bone fragment	0	0	0	0	0	0	0	1	0
Tooth	0	0	0	1	1	4	1	2	0
Jaw palate fragment	0	0	0	0	0	0	0	0	0
Total microfossils	100	100	100	100	100	100	100	100	100
Richness	5	5	6	10	9	12	10	7	2

	NYC35.7	LLDW44.2	LLDW42.3	LLDW36.6	LLDW34.6	LLDW31.3	LD57.8 PLM	
Facies	PLM	SPF	SPF	SPF	SPF	SPF		
Age	Norian	Norian	Norian	Norian	Norian	Norian	Norian	
Foraminifera	1	0	2	1	0	0	0	
Radiolarian	0	0	0	0	0	1	0	
Sphinctozoan sponge	0	0	0	0	0	0	0	
Non-lithistid demosponge spicule	0	4	12	0	1	0	97	
Lithistid demosponge spicule	83	5	0	0	0	0	0	
Hexactinellid spicule	0	0	0	0	0	0	0	
Bryozoan	0	0	0	0	0	1	0	
Brachiopod	0	1	0	0	0	1	0	
Gastropod	0	0	0	0	0	1	0	
Gastropod internal mold	5	5	27	30	46	4	0	
Bivalve	1	1	0	0	0	0	0	
Bivalve fragment	0	12	11	0	0	14	0	
Bivalve internal mold	0	1	0	0	1	35	0	
Cephalopod hooklet	0	0	0	1	0	1	0	
Ammonoid	0	1	0	0	0	0	0	
Ostracod	0	1	0	0	0	0	0	
Echinoderm spine	1	13	16	2	2	1	0	
Echinoderm stereom	0	6	22	48	30	0	0	
Conodont	0	0	0	0	0	1	0	
Denticle	2	5	2	3	2	3	0	
Scale	0	0	0	0	0	0	0	
Scale fragment	1	19	2	2	0	7	3	
Bone fragment	0	23	2	6	8	7	0	
Tooth	6	3	4	7	10	23	0	
Jaw palate fragment	0	0	0	0	0	0	0	
Total microfossils	100	100	100	100	100	100	100	
Richness	8	15	10	9	8	14	2	

fragments). With the exclusion of singletons, there was also a more pronounced negative relationship between echinoderm stereom and vertebrate material (denticles, bones, and scales) (Fig. 5A).

Co-occurrence analysis for the entire dataset using taxonomic microfossil groups was also run excluding singletons (Fig. 5B). When considering only taxonomic classifications, vertebrate material and bivalve material as well as ostracods and hexactinellid sponge spicules tended to co-occur. Hexactinellid sponge spicules and gastropod material tended not to co-occur in samples.

3.4. Mineralogical and taphonomic trends

Several taphonomic remineralization characteristics were observed among the microfossil residues. Most original-carbonate microfossils recovered during manual picking had been altered from their original mineralogy (Table 2). Echinoderm stereom and spines, ostracods, and bivalve fragments recovered were typically silicified (Fig. 6E, F, O). Silicification of original carbonate biominerals was also seen in petrographic thin section both for microfossils and macrofossils. Very small, likely juvenile gastropods and bivalves were preserved as internal molds rather than with original shell mineralogy (Fig. 6H–K). Internal molds

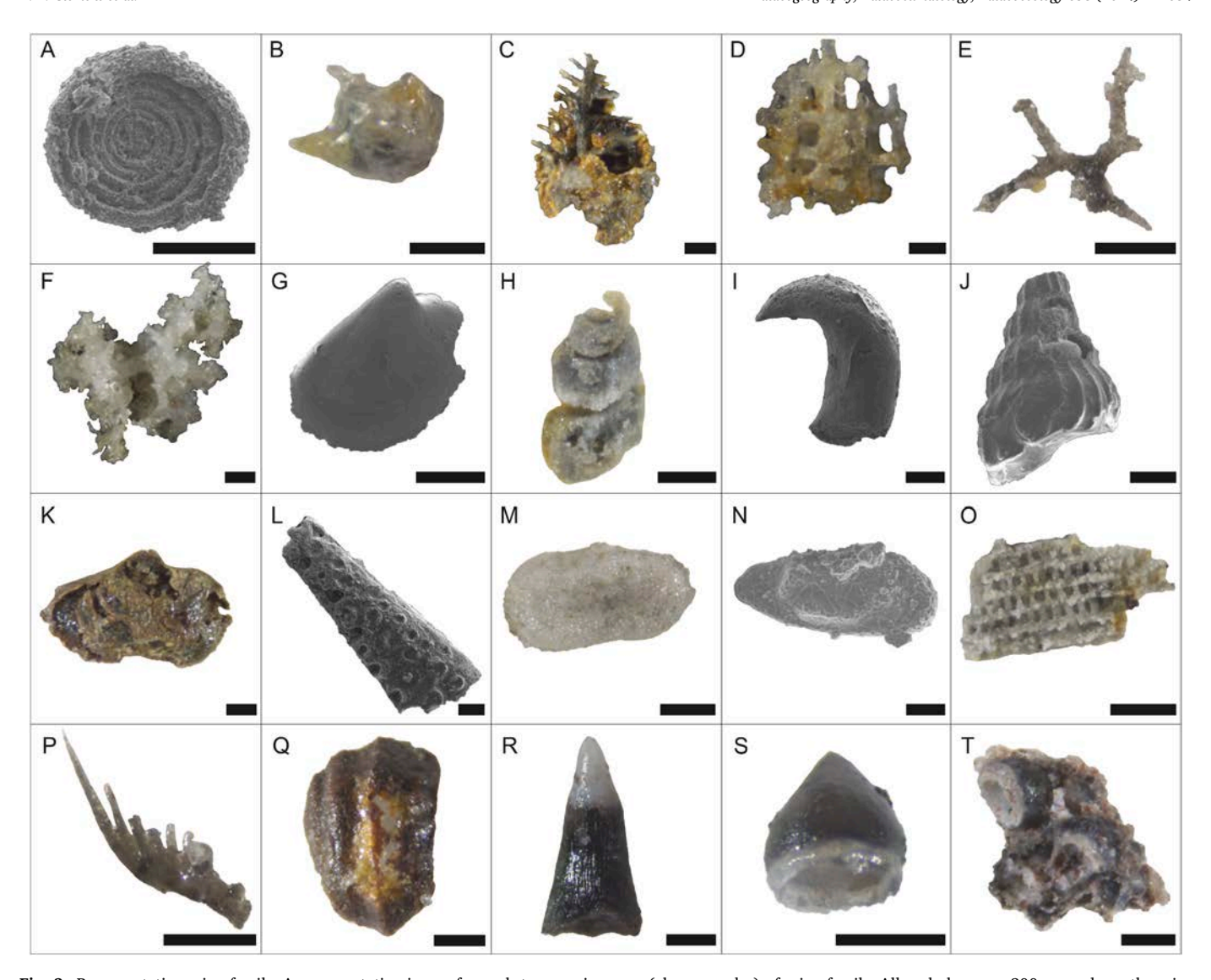


Fig. 2. Representative microfossils. A representative image for each taxonomic group (class or order) of microfossils. All scale bars are 200 µm unless otherwise noted. A) Foraminifera under SEM cf. Ammodiscus, 42.3. B) Radiolaria: cf. Plafkerium, LLDW 31.3. C) Porifera: sphinctozoan sponge fragment NYC, 62.0. D) Porifera: hexactinellid sponge spicule lattice, MT19.9. E) Porifera: non-lithistid demosponge spicule, metaster morphology, WH 6.5. F) Porifera: lithistid demosponge spicule featuring robust overgrowths, WH 26.9. G) Bivalvia: bivalve internal mold under SEM, LLDW 31.3. H) Gastropoda: gastropod internal mold, LLDW 34.6. I) Cephalopoda: cephalopod hooklet under SEM, LLDW 31.3. J) Cephalopoda: juvenile cf. Paracochloceras under SEM, LLDS 44.2. K) Brachiopoda: brachiopod partial shell and internal mold, LLDW 44.2. L) Bryozoa: trepostome bryozoan under SEM, LLDW 31.3. M) Arthropod: ostracod cf. Cavellinidae, MT 17.5. N) Arthropod: ostracod under SEM cf. Bairdiidae, MT 17.5. O) Echinodermata: fragment of stereom texture, LLDW 34.6. P) Chordata: conodont S-element, LLDW 31.3. Q) Vertebrata: dermal denticle, WH 16.7. R) Vertebrata: Saurichthys-type tooth, LLDW 31.3. S) Vertebrata: cf. Sphaerodus tooth, WH 2. T) Vertebrata: cf. Sphaerodus tooth cluster, potential palate, WH 2.

from gastropods and bivalves were often phosphatized (Fig. 6I–K, P), though bivalve internal molds exhibit this mineralogy more often than those of gastropods. Foraminifera were likewise typically silicified or, as in the case of the larger *Ammodiscus* Reuss, 1862 and *Frondicularia* Defrance in d'Orbigny, 1826, preserved as internal molds. Echinoderm spines were observed to be silicified or phosphatized, though rarely in the same sample (Fig. 6E–G, O). Originally silicic and phosphatic microfossils (sponge spicules and vertebrate material, respectively) primarily retained their original mineralogy; however, sponge spicules frequently showed signs of partial dissolution or sugary overgrowths (Fig. 6A–D) and in upper Mount Hyatt Member samples MC 5.9 and MC 8 vertebrate material (primarily teeth) was at least partially pyritized (Fig. 6L–N, Q–R). Pyrite framboids were also observed within the replacement pyrite in microfossil teeth from sample MC 5.9 (Fig. 6M–N, R).

3.5. Taxon-specific trends

3.5.1. Poriferan occurrences through time and between facies

Sponge spicules from non-lithistid demosponges, lithistid demosponges, and hexactinellid sponges varied among facies and through time. While all three identified classifications of sponge spicules can, and do, co-occur in samples, non-lithistid demosponges and lithistid demosponge abundance exhibits an inverse relationship (Table 1, Fig. 7). Samples with common to abundant non-lithistid demosponge spicules (10–97%) tended to not contain common lithistid spicules (<10%) (e.g., MT 2.15, WH 6.5, WH 2, LLDW 42.3, LD 57.8). Similarly, samples with common to abundant lithistid demosponge spicules (10–94%) tended not to contain lithistid demosponge spicules (<10%) (e.g., NYC 35.7, NYC 40, NYC 40.5, NYC 43.6, NYC 65.4, NYC 72.2, NYC 87.6, WH 26.9, WH 32.65). Additionally, when lithistid demosponges are abundant in a sample, they tend to be hyper-abundant, often

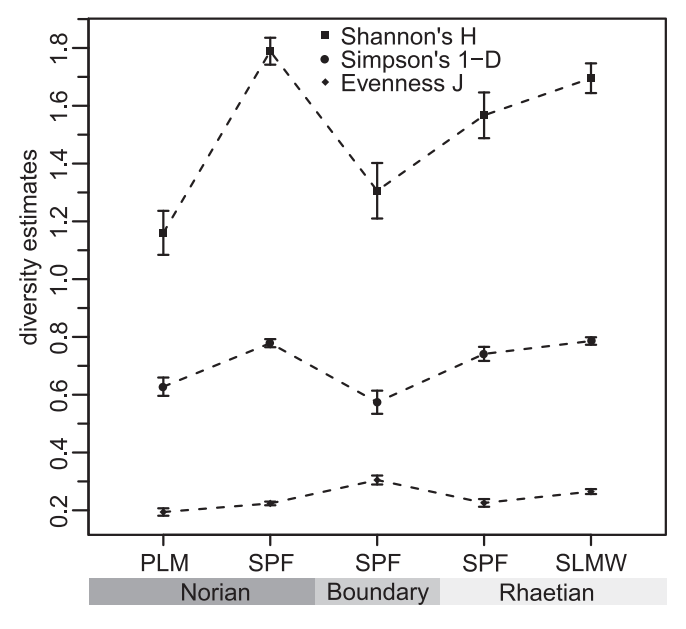


Fig. 3. Microfossil diversity through time and environments. Diversity calculations using Shannon's H, Simpson's 1-D, and Pielou's J (evenness) for Norianage purple lime mudstone facies samples (LD 57.8, NYC 35.7, WH 2, WH6.5) and skeletal packstone–floatstone facies (LLDW 31.3, LLDW 34.6, LLDW 36.6, LLDW 42.3, LLDW 44.2, NYC 40, NYC 40.5, NYC 43.6, NYC 46, NYC 51.4, NYC 54, WH 26.35, WH26.9), Norian–Rhaetian boundary age skeletal packstone–floatstone facies samples (NYC 58.5, NYC58.5b, NYC 61.1, NYC 62, WH 32.4, WH32.65), and Rhaetian-age skeletal packstone–floatstone samples (NYC 66.6, NYC 72.2) and silty lime mudstone–wackestone samples (NYC 87.6, MT2.15, MT 17.5, MT 19.9, MC 5.9, MC 8). Calculations were carried out in R using the *Vegan* package (Oksanen et al., 2020) and 95% confidence intervals were generated using 1000 iterations using the package *Boot* (Davison and Hinkley, 1997; Canty and Ripley, 2021). (For interpretation of the references to color in this figure legend, the reader is referred to the web version of this article.)

comprising 40% or more of the microfossils in a sample (e.g., NYC 35.7, NYC 40, NYC 72.2, NYC 87.6, WH 26.9, WH 32.65).

Sponge spicules showed both time- and facies-specific trends. Nonlithistid demosponge spicules tended to be abundant in the purple lime mudstone facies (PLM) (WH 2, WH 6.5, LD 57.8) except for New York Canyon Road samples where lithistid sponges were abundant in the outer ramp transition facies PLM, the deepest observed facies of the Gabbs Formation. In the skeletal packstone-floatstone (SPF) and silty lime mudstone-wackestone (SLMW) facies, non-lithistid demosponge spicules tend to consistently occur at lower background levels (Table 1, Fig. 7). Both hexactinellid and lithistid sponge spicules are found in facies SPF; however, neither spicule type represents a large component of samples in those facies until the NRB interval, defined by the strontium isotope excursion (SIE) reported in Tackett et al. (2014). This trend of increasing siliceous sponge spicules continues into the Rhaetian-age facies SLMW samples (Fig. 7). This trend is best exemplified by samples from the New York Canyon Road and Windy Hill sections which cross the NRB (Fig. 7).

3.5.2. Echinoderm occurrences through time and between facies

Echinoderm microfossils also showed time- and facies-specific trends. Echinoderm microfossils consist of both echinoid spines and pieces of echinoderm stereom, potentially from echinoids, asteroids, or crinoids. In hand sample and petrographic thin section, echinoderm stereom grains can occasionally be recognizable as crinoid columnals; however, this is rarely possible for the extracted microfossils. Echinoderm spines are present within liberated microfossil assemblages from Norian and Rhaetian-age skeletal packstone–floatstone facies (SPF)

samples in amounts typically <20% and persist in similar amounts (<15%) in Rhaetian-age facies SLMW samples. In contrast, echinoderm stereom can be extremely abundant in Norian-age facies SPF assemblages and may account for >50% of the microfossils picked in a sample (Table 1, Fig. 8). By contrast, in Rhaetian-age facies SPF and SLMW samples, echinoderm stereom never accounts for >46% of a sample and is increasingly rare up-section (Fig. 8, Table 1). Echinoderm stereom abundance also shows a slight negative relationship with bone fragments when considering taphotaxa microfossil groups (i.e. echinoderm stereom and spines separately), but taken together, echinoderm material shares no relationship with vertebrate material generally (Fig. 5).

3.5.3. Vertebrate occurrences through time and between facies

Vertebrate microfossils, consisting of teeth, scale fragments, bone fragments, and chondrichthyan denticles, also display time and facies trends. Teeth from Severnichthys acuminatus (Agassiz, 1843) and cf. Sphaerodus Agassiz, 1833 were identified as well as denticles (Fig. 20–T). Vertebrate microfossils were observed in acid residues from all studied facies (SLMW, SPF, and PLM) and from all sample locations; however, samples from New York Canyon Road had little vertebrate material of any kind. Vertebrate microfossils, particularly teeth, scale fragments, and bone fragments were common to abundant in inner ramp transition facies SLMW (often 30-60%) and were increasingly abundant up-section. In mid-ramp facies SPF, vertebrate material typically accounted for 10-20% of the microfossils but could reach as high as 56% (Table 1). Sample WH 2 in facies PLM also displayed a high abundance of vertebrate microfossils (73%); however, 53% of the sample was the same type of cf. Sphaerodus tooth (Fig. 2S-T). Many of these teeth were still articulated into an oriented cluster, possibly fragments of a dental palate (Fig. 2T) and potentially indicating proximity to a partiallyarticulated actinopterygian fossil. For this reason, WH 2 is not considered representative of vertebrate material distributed within facies PLM.

4. Discussion

4.1. Facies heterogeneity

The facies model proposed for the Gabbs Formation consists of simple facies belts, largely owing to the limited exposure of the formation (Clement and Tackett, 2021); however, modern shallow marine systems rarely produce such simple patterns. Though broad interpretation of environments based on the depth profiles can produce large facies belts, along these belts facies tend to be heterogeneous (Read, 1985). This is often exemplified in basin analysis by combining both parallel to dip and parallel to strike profiles into more cohesive coastline facies models. The limited exposure of the Gabbs Formation makes such nuance difficult, but the variability of microfossil assemblages, both with time and among localities, aids in the description of facies and their variability within the facies model.

In the Gabbs Formation, the microfossil assemblages varied greatly within the skeletal packstone-floatstone (SPF) and silty lime mudstone-wackestone (SLMW) facies and among sample localities. Cluster analysis based on the taxonomic microfossil assemblages showed sample groupings based on hyper-abundant microfossils which often followed specific facies and locality patterns (Fig. 4A). For instance, of the samples that were > 40% stereom, primarily found in the skeletal packstone-floatstone (SPF) facies, samples from New York Canyon Road tended to group together, implying that the locality is more similar to itself than other SPF facies samples across the study area and through time (Fig. 4A). Likewise, silty lime mudstone-wackestone (SLMW) facies from the Mine Test locality grouped together owing to their abundance of ostracod microfossils, thus differentiating them from other facies SLMW samples from Muller Canyon and New York Canyon Road. Considering the variation within facies, microfossil assemblages could not be reliably used to describe facies SPF and SLMW.

The outer ramp-transition purple lime mudstone (PLM) facies also

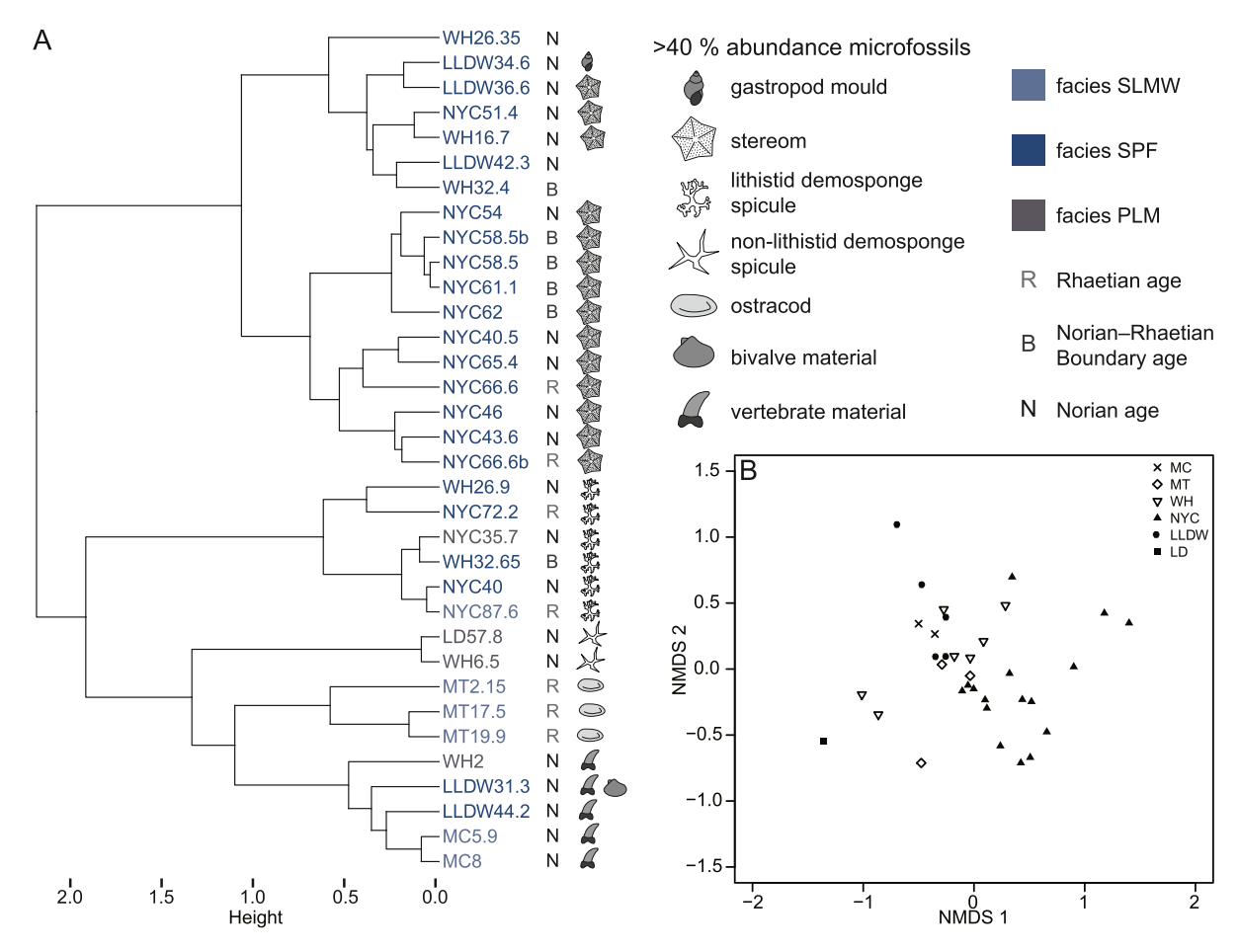


Fig. 4. Cluster and NMDS analysis of microfossil assemblages. A) Cluster analysis of microfossil samples. Sample names are color-coded by facies and symbols indicate the stage and dominant microfossil. B. NMDS analysis of microfossil samples labeled according to locality.

showed differences among sample localities but was characterized by an abundance of lithistid and non-lithistid demosponge spicules. Lithistid demosponge spicules are highly abundant in facies PLM samples from New York Canyon Road and non-lithistid demosponge spicules dominate facies PLM samples from Windy Hill and Luning Draw, with the exception of sample WH 2. In modern settings, both lithistid and nonlithistid demosponges often occupy a wide range of depths, especially deeper environments similar to facies PLM (Maldonado et al., 2016; Alvarez et al., 2017). Their dominance in facies PLM at multiple localities may therefore be seen as typical for this system. Non-lithistid demosponges remained a steady background component of the assemblages in facies SPF, typically comprising 0-12% of the sample. The resurgence of lithistid demosponge spicules up-section in mid ramp facies SPF, also previously a minor component, is potentially indicative of changes in dissolved silica (DSi) availability in shallower environments rather than taphonomic change as non-lithistid demosponge spicules from the same samples do not increase. In sample WH 2, over half of the microfossils were the same type of tooth, implying that the rock digested for this sample may have contained a partial fish jaw palate rather than shed teeth of fish and sharks in these environments.

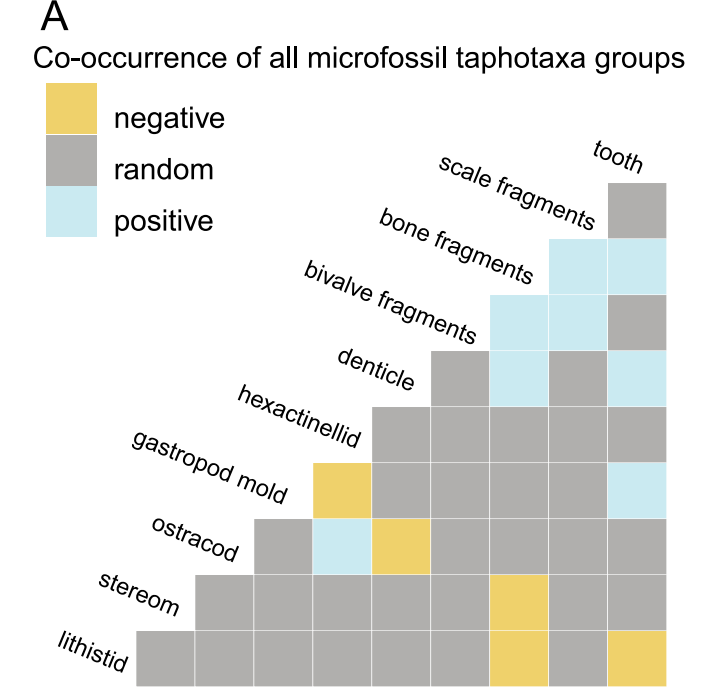
Microfossil assemblages in facies SPF, SLMW, and PLM demonstrate the presence of environmental heterogeneity across the Upper Triassic carbonate ramp. These patterns emerge both spatially among measured sections in all facies and through time in the case of facies SPF in the New York Canyon Road locality.

4.2. Tracking silica fluctuations from the late Triassic through the early .hrrassic

In the Gabbs Formation, hypersilicified sponge spicules are mainly limited to the outer ramp transition facies in Norian deposits but become common in shallower deposits of Rhaetian-age. Silica fluxes in the latest Triassic are illustrated by an abundance of silica-limited microfossils across the Norian–Rhaetian boundary (NRB) and widespread silicification of original-carbonate microfossils. Dissolved silica (DSi or silicic acid) in ocean basins may shift as a result of changing rates of basalt erosion, as basalt erodes more rapidly than typical continental rocks (Dessert et al., 2003) and yields much higher dissolved silica as a result (Hartmann et al., 2010). Strontium isotopes are a valuable proxy for volcanic activity (Korte and Ullmann, 2018), which are recorded with high fidelity in calcareous biominerals. Here, we consider silica and strontium isotope fluctuations in the context of biogenic sediments from the New York Canyon region.

4.2.1. Sponge spicules as an indicator of dissolved silica

In the Early Mesozoic, sponges and radiolarians constituted the largest demand and sink of DSi prior to the evolution and radiation of diatoms (Tréguer et al., 1995; Maldonado et al., 2011, 2019). Planktonic production of biogenic silica, by radiolarians and diatoms, dominates the modern ocean silicon cycle, accounting for at least five times the estimated output of biogenic silica from sponges (Tréguer et al., 2021). The planktonic production and subsequent burial of biogenic silica is the cause of depleted global DSi concentrations beginning after the evolution and expansion of diatoms in the Cretaceous–Paleogene (Maldonado et al., 2011). Sponges have higher DSi saturation requirements than



B Co-occurrence of microfossil taxonomic groups

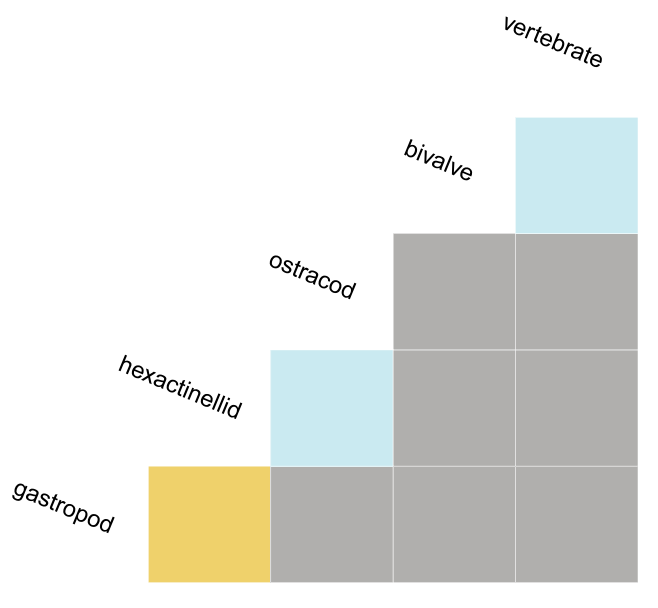


Fig. 5. Co-occurrences of microfossils. A) Co-occurrence of microfossils grouped by taxonomic and taphonomic characteristics (taphotaxa). B) Co-occurrence of microfossils grouped by taxonomy.

diatoms for biomineralization, making modern sponges a smaller silicon sink in DSi-depleted shallow-water environments, and remain a significant silicon reservoir in deep aphotic environments that exhibit higher DSi than in shallow marine environments (Maldonado et al., 2011, 2019; Uriz et al., 2003). Without this modern depletion in DSi and competition from diatoms, sponges were likely a primary driver of the ocean silica cycle in the Early Mesozoic (Tréguer et al., 1995, Maldonado et al., 2011, 2019).

Hyper-silicifying sponges, such as hexactinellids, still show a preference in modern oceans for environments with higher DSi

concentrations (Maldonado et al., 2016; Alvarez et al., 2017), despite modern sponges' ability to grow and fix silica in DSi-depleted waters (Uriz et al., 2003; Maldonado et al., 2019; Tréguer et al., 2021). Hexactinellid sponges create rigid, hypersilicified lattice skeletons and are most often found in modern cool, non-turbid, deeper-water environments, likely due to higher DSi concentrations and requirements for feeding strategies (Uriz et al., 2003; Levs et al., 2007). In these environments, hexactinellid sponge grounds and bioherms constitute major biogenic silica reservoirs and contribute to the recycling of silicon through DSi released from shallowly buried spicules (Maldonado et al., 2019, 2021; Tréguer et al., 2021), and possibly support new sponge populations with locally increased DSi (Maldonado et al., 2021). Modern hexactinellid sponges are also rarely found in shallow water (<20 m) in Antarctica, Southern New Zealand, submarine caves in the Mediterranean, and coastal areas of the North Pacific (Leys et al., 2007) where surface (<50 m depth) concentration of DSi are elevated (Cermeño et al., 2015). This indicates that while hexactinellid sponges can and do occupy shallower marine environments, they thrive at elevated DSi levels, and in large numbers may be a useful proxy for higher DSi concentrations in ancient shallow marine settings. Thus, the presence and abundance of intact spicules from dense hyper-silicifying sponges, such as hexactinellid sponges and lithistid demosponges, may represent an influential sink of biogenic silica and both a source and proxy indicator of increased DSi in the Triassic and Jurassic.

4.2.2. Silicification as an indicator of dissolved silica

The silicification observed in petrographic thin sections and liberated microfossils extracted from samples suggests high pore water mobility of DSi through the NRB interval, as defined by the strontium isotope excursion (SIE). Silicification of carbonate material typically requires fluids that are silica-saturated and slightly acidic as well as a susceptible ultrastructure within the carbonate fossil and can be accelerated by the decay of organic matter (Butts, 2014). The partial silicification of the echinoderm and bivalve material is granular chalcedony, and in echinoderm stereom it preserves detailed structure indicating that silicification likely occurred in shallowly buried sediments during early diagenesis. Delicate silicified rims that likely surrounded calcite fossils, also found in the acid residues of the samples, support early silicification as these may form during the decay of organic matter (Butts, 2014). A convenient candidate source for pore water silica during early diagenesis was the sponge spicules in surrounding sediments, owing to the rapid rate of dissolution for biogenic silica compared to quartz (Van Cappellen et al., 2002; Butts and Briggs, 2011; Quéguiner, 2016) and the nearly ubiquitous presence of sponge spicules in samples. While multiple sources of localized silicification can influence fossil preservation, such as nearby hydrothermal activity, stratigraphic control was observed on silicification in and above beds rich in lithistid and non-lithistid sponge spicules in facies SPF, which suggests a relationship (Table 2). The stratigrahic control of silicification also implies that silicification was not due to later diagenesis that may have impacted the entire Gabbs Formation. The evidence for early silicification and presence of intact sponge spicules indicates that sponge spicules may have been sufficiently abundant to saturate pore waters without being entirely dissolved. In this way, the silicification of microfossils in the Gabbs Formation may provide a proxy for tracking the pore water DSi availability through the NRB.

4.2.3. Implications for the silica cycle through the Norian–Rhaetian boundary

The microfossil assemblages of the Gabbs Formation show a marked increase in hypersilicified sponge spicules in mid-ramp environments across the NRB, reminiscent of sponge communities of the Lower Jurassic (Ritterbush et al., 2014, 2016). Recent work by Ritterbush et al. (2014, 2016) and Clement et al. (2020) has established that the New York Canyon area experienced elevated DSi levels in the Lower Jurassic (Hettangian–Sinemurian); the primary evidence for which includes the

Table 2Taphonomy of microfossil assemblages.

	SC	PhC	PyC	С	MC	MNC	MPh	S	Ph	PyPh	PhO
MC8	28	0	3	0	0	0	0	5	63	1	0
MC5.9	9	8	4	0	0	0	18	1	36	24	0
MT19.9	54	1	0	0	0	0	0	20	25	0	0
MT17.5	63	4	0	0	0	0	0	3	30	0	0
MT2.15	78	0	0	0	0	0	0	21	1	0	0
NYC87.6	0	0	0	0	0	0	0	100	0	0	0
NYC72.2	19	0	0	0	0	0	0	81	0	0	0
NYC66.6b	77	0	0	0	0	0	0	14	9	0	0
NYC66.6	47	0	0	1	0	4	0	48	0	0	0
WH32.65	9	1	0	0	0	1	0	85	4	0	0
WH32.4	48	6	0	0	0	16	9	12	9	0	0
WH26.9	29	2	0	0	0	11	1	46	11	0	0
WH26.35	53	1	0	0	0	33	1	1	11	0	0
WH16.7	65	2	0	0	0	19	2	1	11	0	0
WH6.5	2	1	0	0	0	0	1	87	9	0	0
WH2	0	2	0	0	0	0	0	24	74	0	0
NYC65.4	58	0	0	0	0	0	0	40	2	0	0
NYC62	63	15	0	0	0	0	0	22	0	0	0
NYC61.1	92	0	0	0	0	0	0	8	0	0	0
NYC58.5b	94	0	0	0	0	0	0	6	0	0	0
NYC58.5	94	0	0	0	0	0	0	6	0	0	0
NYC54	85	0	0	0	0	13	0	1	1	0	0
NYC51.4	67	3	0	0	0	17	2	6	5	0	0
NYC46	64	3	0	0	0	12	6	10	5	0	0
NYC43.6	84	2	0	0	0	1	0	12	1	0	0
NYC40.5	60	7	0	1	0	4	4	21	3	0	0
NYC40	6	0	0	0	0	0	0	94	0	0	0
NYC35.7	4	0	0	0	0	0	5	84	7	0	0
LLDW44.2	22	13	0	0	0	1	5	9	50	0	0
LLDW42.3	31	21	0	0	0	8	18	12	10	0	0
LLDW36.6	51	0	0	0	0	30	0	0	18	0	1
LLDW34.6	31	0	0	1	1	42	4	1	20	0	0
LLDW31.3	16	0	0	0	0	1	40	1	41	0	1
LD57.8	0	0	0	0	0	0	0	97	3	0	0

Table 2. Taphonomy of microfossil assemblages. Taphonomic categories: SC- silicified originally carbonate, PhC- phosphatized originally carbonate, PhC- phosphatized originally carbonate, C- original or remineralized carbonate, MC- internal mold of carbonate, MNC- internal mold of non-carbonate, MPh- internal mold of phosphate, S- original silica, Ph- original phosphate (apatite), PyPh- pyritized originally phosphate, PhO- phosphatized originally organic or chitin.

proliferation of a sponge ramp over the uppermost Triassic carbonate-dominated ramp (Ritterbush et al., 2014, 2016), and the observation of iron-clay ooids as a condensation feature in otherwise carbonate rocks (Ritterbush et al., 2016; Clement et al., 2020). Through the sampling of microfossil assemblages, which detects the presence of both biogenic silica sponge spicules and secondary silicification, similar evidence for elevated DSi was uncovered for strata across the NRB.

The poriferan spicule record through the NRB exhibits increased abundance of hexactinellid and lithistid sponge spicules indicating ample availability of water column DSi. The increase in hypersilicified spicules from the NRB and early Rhaetian occurs in mid-ramp to inner ramp transition environments, represented by facies SPF (skeletal packstone-floatstone) and SLMW (silty lime mudstone-wackestone) respectively. The record of sponge spicules is best exemplified in the New York Canyon Road measured section where ⁸⁷Sr/⁸⁶Sr records can be used to accurately identify the stratigraphic location of the NRB (Tackett et al., 2014). Below the NRB at New York Canyon Road, lithistid demosponge spicules are the dominant microfossil in the deepest environments, represented by facies PLM; however, in mid-ramp facies (SPF) prior to the NRB hypersilicified lithistid demosponge and hexactinellid sponge spicules are rare to absent (Fig. 7A), though nonlithistid demosponges are present. This observation is consistent with the interpretation that in the Norian only deeper environments contained the DSi needed to sustain larger sponge communities. Across the NRB in mid-ramp environments there is an increase in both hexactinellid and lithistid demosponge spicules at New York Canyon Road (Fig. 7A). This trend continues into the early Rhaetian where hypersilicified spicules often account for >30% of a microfossil sample. The resurgence of sponge material in New York Canyon Road samples is echoed in the Windy Hill samples where all sponge spicules are rare to absent in facies

SPF during the Norian, followed by the sudden appearance of lithistid demosponge spicules at the NRB (Fig. 7B). The sudden appearance of abundant lithistid demosponge and hexactinellid sponge spicules in mid-ramp facies SPF at the NRB indicates that DSi became sufficiently elevated in shallower environments to sustain greater silicon demands of hyper-silicifying sponges. While not as marked of a shift in DSi as observed from development of a glass ramp in the Early Jurassic (Ritterbush et al., 2014, 2016), the appearance of abundant hypersilicified sponge spicules across the NRB and in lower Rhaetian sediments indicate fluctuations in bottom water DSi increasing throughout the Late Triassic.

Silicification of carbonate microfossils is most common in mid-ramp facies SPF during the late Norian and through the NRB. Silicification likely occurred early during shallow burial owing to the partial replacement of bivalve shell material by very fine-grained chalcedony and the detailed partial replacement of stereom. The source of pore water DSi in the upper Norian mid-ramp deposits was likely from sponge spicules. Sponge spicules are thermodynamically susceptible to dissolution during early burial, and early dissolution may have emphasized the rarity of sponge spicules in Norian mid-ramp samples. The relative abundance of non-lithistid demosponge spicules remained consistent into the early Rhaetian (Fig. 7), indicating that while early dissolution may have impacted the spicule record, the signal of increased hypersilicified spicules across the NRB is real and potentially even reduced. The silicification of calcite remained common across the NRB in facies SPF as hyper-silicifying sponges appeared in mid-ramp environments indicating a higher availability of DSi in the water column as well as pore water (Fig. 9). Silicified calcite is also present in the early Rhaetian, though it accounts for less of the microfossil assemblage than in the Norian. Rhaetian silicification indicates pore water DSi availability was

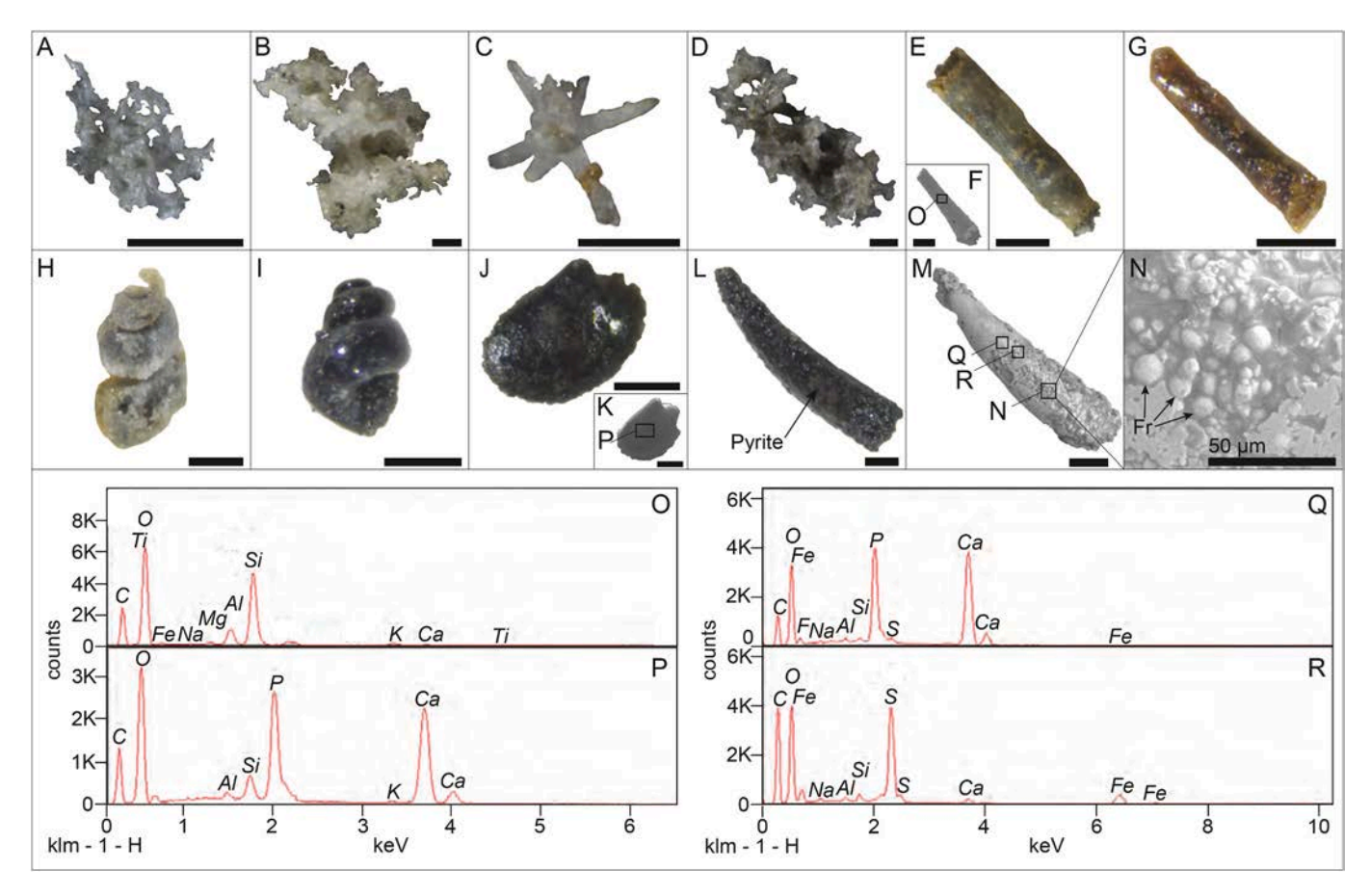


Fig. 6. Microfossil taphonomy. A) Delicate lithistid demosponge spicule, NYC 35.7. B) Robust lithistid demosponge spicule, WH 26.9. C) Isolated hexactinellid spicule fragment, NYC 46. D) Overgrown hexactinellid spicule lattice, NYC 62. E) Silicified echinoderm spine, NYC 51.4. F) Silicified echinoderm spire under SEM, WH 26.35. G) Phosphatized echinoderm spine, LLDW 44.2. H) Silicified gastropod internal mold, LLDW 34.6. I) Phosphatized gastropod internal mold, LLDW 31.3. J) Phosphatized bivalve internal mold, LLDW 31.3. K) Phosphatized bivalve internal mold under SEM, LLDW 31.3. L) cf. *Gyrolepis* tooth showing partial dissolution of apatite and pyrite replacement, MC 5.9. M) cf. *Gyrolepis* tooth under SEM showing partial dissolution of original apatite, pyrite replacement, and pyrite framboids pictured in (N), MC 5.9. N) Pyrite framboids (Fr) in dissolved sections of M, MC 5.9. O) EDS analysis for box 1 indicated in F, WH 26.35. P) EDS analysis for box 2 indicated in K, LLDW 31.3. Q) EDS analysis for box 3 indicated in M, MC 5.9. R) EDS analysis for box 4 indicated in M, MC 5.9.

likely maintained; however, a decrease in carbonate taxa may contribute to the decline in silicified carbonate microfossils in facies SLMW.

The increased availability of DSi in the latest Rhaetian and through the Early Jurassic is likely related to the weathering of basalt deposits from major tectonic rifting events also proposed to have induced global warming and ocean acidification (CAMP volcanism) given the influence of continental weathering on the global silica cycle, the concurrent decrease in the strontium isotope ratios, and the unique suite of diagenetic and paleontological associated features (Tréguer et al., 1995; Greene et al., 2012; Pálfy and Kocsis, 2014; Ritterbush et al., 2014, 2016; Korte et al., 2019); however, some proxies for volcanic activity suggest an earlier phase for hydrothermal or basaltic input to marine systems across the NRB (Zaffani et al., 2017). Large injections of CO₂ from CAMP volcanism are tracked by negative δ^{13} C excursions as well as the results of silicate weathering of the deposits themselves (Greene et al., 2012; Schaller et al., 2012; Bachan and Payne, 2016; Korte et al., 2019). Zaffani et al. (2017) and Rigo et al. (2020) recognize similar carbon cycle perturbations during the late Norian through the Rhaetian, interpreted as emplacements of earlier large igneous provinces (LIP). This interpretation is supported by strontium isotope records. Weathering of basalt also releases non-radiogenic 86Sr resulting in lower $^{87}\mathrm{Sr}/^{86}\mathrm{Sr}$ seawater values that can be seen across the NRB as well as the TJB (in association with CAMP volcanism) (Korte et al., 2003; McArthur et al., 2012; Callegaro et al., 2012; Lindström et al., 2021). The weathering of silicate minerals in hydrothermal or basaltic deposits, associated with 87Sr/86Sr, from earlier late Norian and Rhaetian-age

LIPs may therefore have also supplied the NRB with increased DSi availability concurrent with the observed increase in mid-ramp hypersilicified sponge spicules.

This study establishes the presence and opportunism of hypersilicifying sponges in the mid-ramp facies of the Upper Triassic carbonate ramp prior to their main proliferation in the Lower Jurassic (Ritterbush et al., 2014, 2016). Whole sponges are not commonly found in macrofossil studies of the Upper Triassic deposits and have largely gone unreported as a component of the benthic community in the Gabbs Formation (Laws, 1978, 1982; Tackett and Bottjer, 2016), and can be difficult to discern in petrographic thin section analysis due to rarity or silicification. Their presence is easily detectable, however, through buffered acid extraction microfossil surveys. The rare but persistent presence of non-lithistid demosponges in the outer ramp to inner-ramp transition facies of the Upper Triassic carbonate ramp is expected as demosponges often inhabit shallower and less silica-rich environments than hyper-silicifying sponges (Maldonado et al., 1999). Finding spicules of hyper-silicifying sponges (lithistid demosponges and hexactinellid sponges) in these environments that coincide with the negative strontium isotope excursion at the NRB demonstrate the tendency toward opportunism in these groups to rapidly move into shallower facies during periods of elevated DSi. This feature of the sponge community in the New York Canyon area is best exemplified by the proliferation of a sponge-dominated glass ramp in the Lower Jurassic described by Ritterbush et al. (2014, 2016) where elevated DSi and the collapse of the carbonate benthos allowed the sponge community to

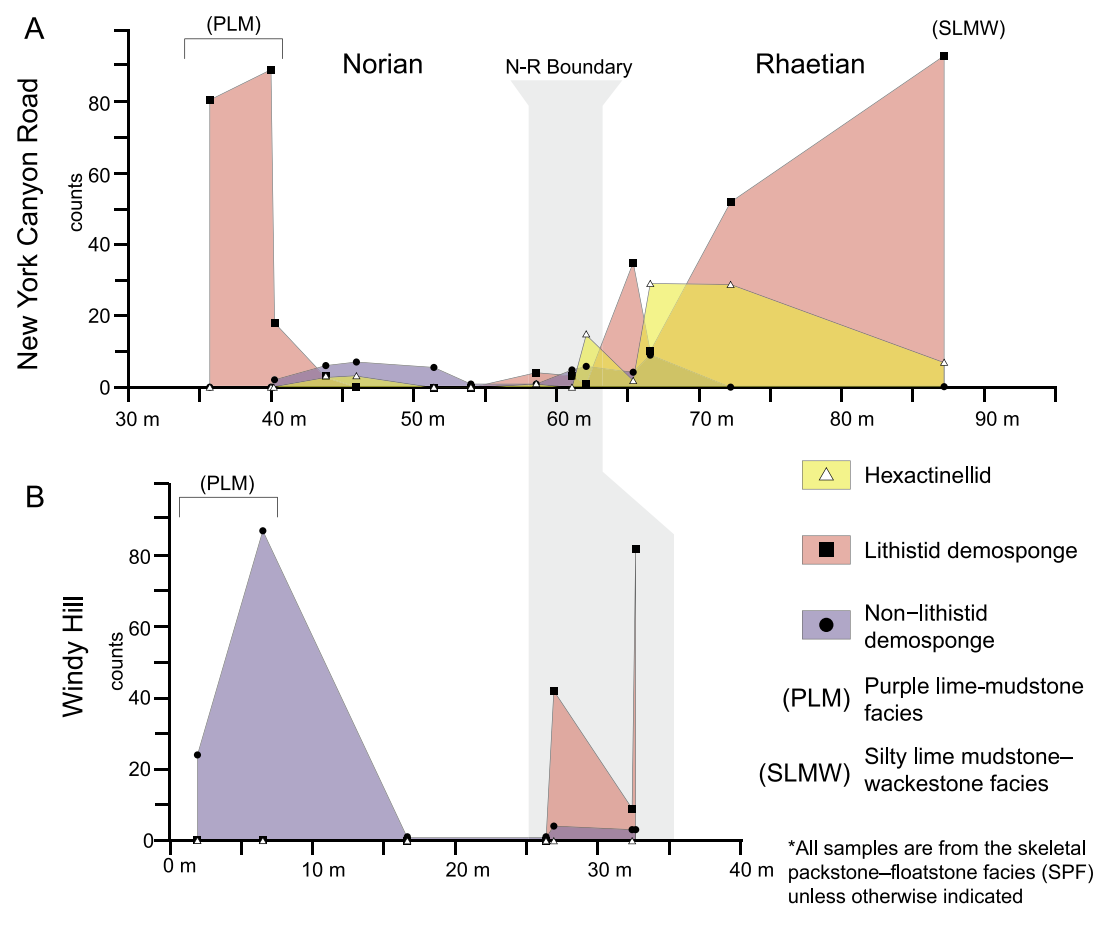


Fig. 7. Sponge material plotted by stratigraphic position. A) Hexactinellid, lithistid demosponge, and non-lithistid demosponge material from the New York Canyon Road locality plotted by stratigraphic position. B) Hexactinellid, lithistid demosponge, and non-lithistid demosponge material from the Windy Hill locality plotted by stratigraphic position.

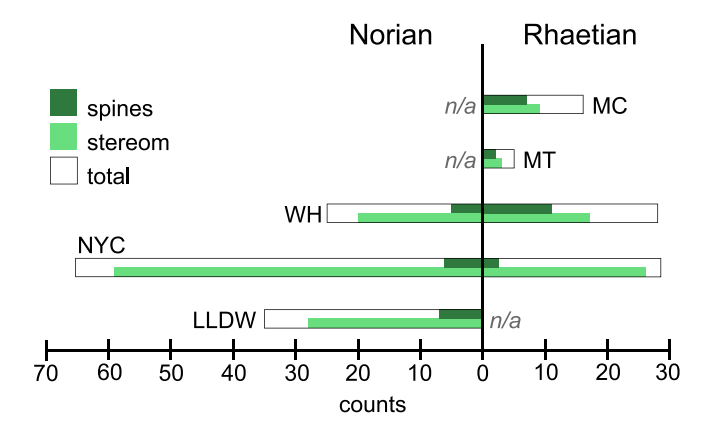


Fig. 8. Echinoderm material proportions through time. Counts are based on assemblages from localities Lower Luning Draw West, New York Canyon Road, Windy Hill, Mine Test, and Muller Canyon.

flourish.

4.3. Tracking shifts in redox conditions during the latest Triassic with taphonomic characteristics

The microfossil survey of the Gabbs formation shows variability in the preservation style of several taxonomic groups of microfossils, most notably echinoderms, molluscan internal molds, and vertebrate groups. While some fluctuation in taphonomy is most likely due to slight geochemical changes coinciding with minor condensation at flooding surfaces (Kidwell, 1989; Föllmi, 2016), we conclude that some broad trends across sample locations and through time are more suggestive of changes in benthic redox conditions across the carbonate ramp environment.

4.3.1. Evidence for acidification prior to the Triassic-Jurassic boundary in the New York Canyon region

The changes in microfossil assemblages and preservation across the NRB have important implications for how the TJB up-section is interpreted. Environmental upheavals including warming and acidification are likely to have intensified toward the end of the Triassic Period, contributing to the mass extinction, but some recent studies suggest that marine environments may have been deteriorating nearly continuously from the NRB through to the end of the Triassic (Zaffani et al., 2017, 2018; Rigo et al., 2020; Schoepfer et al., 2022). Multiple global localities for the TJB, including New York Canyon, exhibit a negative stable carbon isotope excursion (CIE) that is considered to be associated with a large injection of CO2 and acidifying conditions immediately prior to the boundary (Greene et al., 2012; Korte et al., 2019). New York Canyon represents an important example of a persistent carbonate deposition on a mixed carbonate-siliciclastic ramp from the Norian through the TJB (Ritterbush et al., 2016; Clement and Tackett, 2021). The well-defined facies succession leading up to this extinction in the New York Canyon region presents an excellent opportunity to characterize environmental shifts in early Rhaetian environments as well.

In the Gabbs Formation of the New York Canyon region, the facies and stratigraphic analysis in Clement and Tackett (2021) showed that

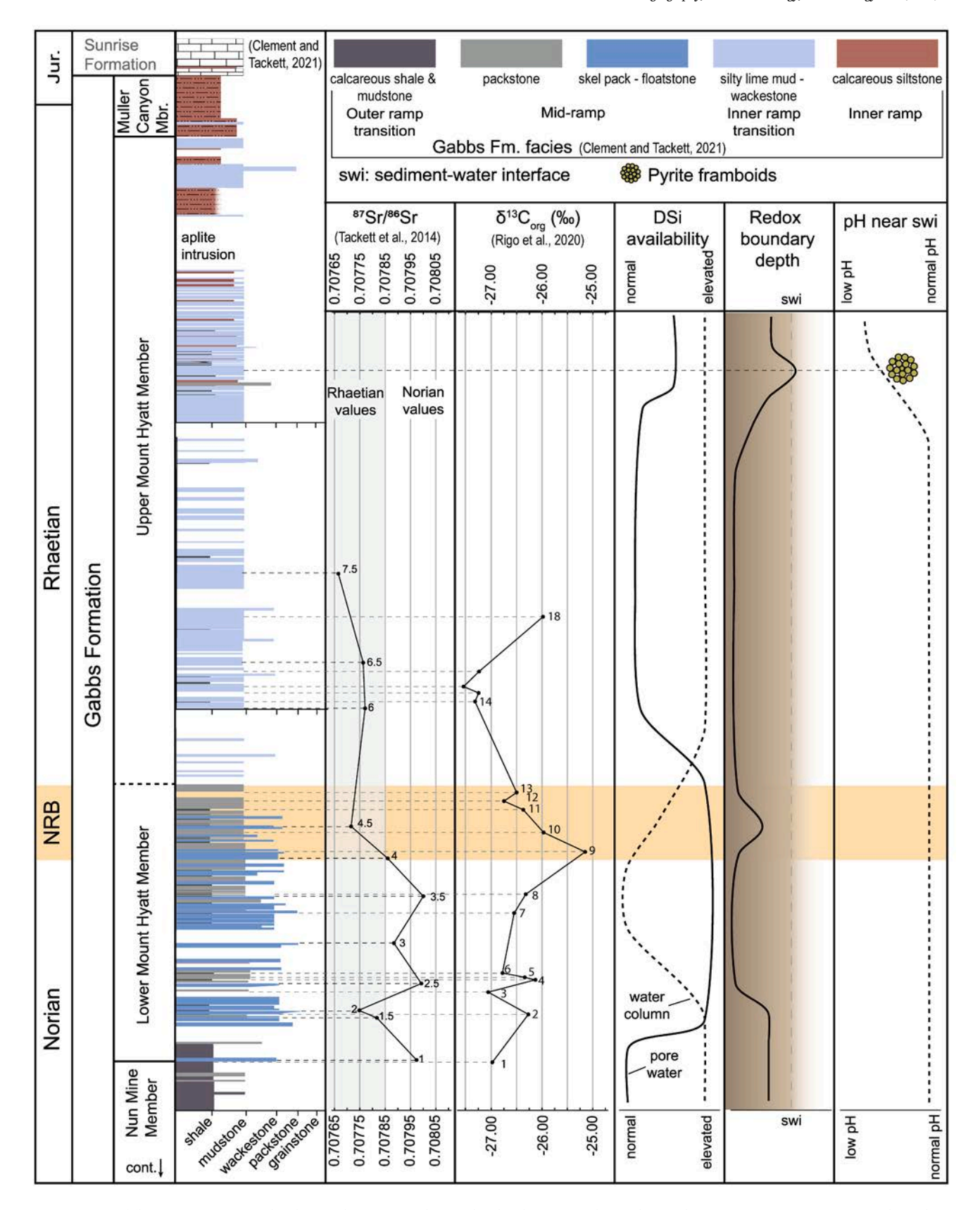


Fig. 9. Summary of fluctuations in DSi and redox conditions coincident with other known geochemical perturbations. Representative stratigraphic column is a combination of the stratigraphy measured at New York Canyon Road and Muller Canyon reproduced with permission from Clement and Tackett (2021).

the loss of carbonate facies up-section from the Mount Hyatt Member to the Muller Canyon Member is a poor proxy for the onset of acidification indicated by the stratigraphically higher, mass extinction-associated negative CIE. The facies transition from the silty lime mudstone–wackestone (SLMW) facies to the calcareous siltstone (CSt) facies is gradual and begins as low as 35 m below the extinction interval and the final loss of carbonate facies, implying that the calcareous siltstone beds that contain the extinction interval itself (as well as the TJB) represent a predictable facies shift, not a result of carbonate non-deposition owing to acidifying conditions (Clement and Tackett, 2021). Therefore, better fossil or geochemical evidence must be used to identify the onset of acidification.

Geochemical evidence of acidification immediately prior to the negative CIE associated with the extinction interval is well-documented by Larina et al. (2021) through a precursor negative CIE followed by increased percent goethite coupled with an increase in the ratio of mercury to total organic carbon and a progressive decrease in macrofossil abundance up to three meters below the extinction interval. While these data suggest the effects of acidifying conditions in beds of the calcareous siltstone facies (CSt) in the lower Muller Canyon Member, after the loss of fully-carbonate facies, it does not give an indication of the conditions during most of the Rhaetian and the potential earliest onset of acidification. Likewise, $\delta^{13}C_{\text{org}}$ values reported in Rigo et al. (2020) for the Mount Hyatt Member show a negative CIE at the NRB, a distinct isotopic event from the CIE that is interpreted to mark the onset of the end-Triassic mass extinction interval. This newly-recognized negative CIE at the NRB has not previously been considered in the context of associated geochemical or ecological changes; however, biosediment abundance and taphonomic patters across the NRB may reveal links to environmental changes. Thus, the Rhaetian Stage may have hosted a series of environmental shifts that shifted the carbon pool and contributed to the high degree of faunal turnover between the Triassic and Jurassic and requires a higher-resolution geochemical and paleontological investigation to characterize seafloor redox conditions during an interval of paleoecological change (Tackett and Bottjer, 2016; Laws, 1978, 1982) leading up to a mass extinction.

4.3.2. The role of dysoxia and acidification in phosphatization and pyritization

The differential preservation of microfossil assemblages between the lower and upper Mount Hyatt Member provides a unique opportunity to track more subtle changes in redox conditions via the preservation of phosphate and pyrite not easily captured by macrofossil or bulk lithologic samples. Both phosphatization and pyritization of fossils can indicate altered redox and pH conditions in pore waters (Briggs et al., 1993; Sawlowicz, 1993; Briggs and Wilby, 1996; Wignall and Newton, 1998; Briggs, 2003; Schoonen, 2004; Dornbos, 2011), and both are observed to systematically increase in the upper Mount Hyatt Member of the Gabbs Formation. Phosphate-preserving environments are typically characterized by low sedimentation and high primary productivity, providing an influx of organic material and near-neutral sediment pore waters (Föllmi, 1996; Dornbos, 2011), resulting in the common occurrence of originally phosphate and phosphatized fossils in distal facies and condensed sections, such as on flooding surfaces (Catuneanu, 2006; Föllmi, 2016). A slight reduction in pore water pH to around 7 destabilizes calcium carbonate and allows for the precipitation of phosphate from saturated pore water often in dysoxic conditions (Briggs et al., 1993; Briggs and Wilby, 1996; Briggs, 2003; Dornbos, 2011). Though not a direct indication of acidification or dysoxia at the sediment-water interface, an abundance of phosphatized organic (e.g., coprolites and chiton) or calcium carbonate fossils indicate lowered pH conditions and potentially lower oxygenation within sedimentary pore waters (Briggs et al., 1993; Briggs and Wilby, 1996; Briggs, 2003; Dornbos, 2011; Gueriau et al., 2020). When coupled with other indicators, such as a decline of other remineralized carbonate fossils and pyritization of fossils, phosphatization of microfossils outside of distal or

condensed deposits could be a useful indication of lowered pH in the Mount Hyatt Member facies.

The pyritization of phosphatic fossils indicates an even narrower range of depositional redox conditions than that of phosphatized organic and carbonate fossils. The precipitation of sedimentary pyrite requires reducing, and often anoxic, conditions as well as a source of dissolved sulfide and ferrous iron (Sawlowicz, 1993; Wilkin et al., 1996; Schoonen, 2004). The decay of organic matter on the seafloor and in shallow sediments consumes oxygen and provides a source of energy for sulfate reducing bacteria to produce the necessary dissolved sulfide byproducts and can promote the local pyritization of organic material (Shawar et al., 2018; Rickard, 2019). Owing to these parameters, sedimentary pyrite is often associated with dysoxic conditions in pore waters (Sawlowicz, 1993; Wignall and Newton, 1998; Schoonen, 2004). Pyrite framboids, spherical aggregates of micron to submicron-sized pyrite grains (Sawlowicz, 1993), are considered largely syndepositional or very early diagenetic, their formation limited to below the redox boundary near the sediment-water interface or within the water column during euxinic conditions (Wilkin et al., 1996; Wignall and Newton, 1998; Rickard, 2019); therefore, the presence of pyrite framboids has often been associated with sediment-water interface and even water column anoxia in the rock record (Wignall and Newton, 1998; Wignall et al., 2005; Gallego-Torres et al., 2015; Huang et al., 2017, Emmings et al., 2022; Li et al., 2022; and others). The replacement of originally phosphatic(apatite) fossils (such as teeth and denticles) with pyrite also implies dysoxic conditions and a lowered pH, necessary to destabilize apatite, within the shallow pore waters during early diagenesis (Brett and Baird, 1986; Guidry and Mackenzie, 2003; Rickard, 2019). The presence of pyritized, formerly apatite, microfossils (e.g., teeth) and pyrite framboids in a sample therefore indicates likely shallow pore water dysoxia and low pH that may have extended to the sedimentwater interface.

Given the geochemical conditions of their formation, associations of phosphatized, pyritized, and silicified microfossils along with un-altered microfossils in a sample may be used as a proxy for redox conditions at or near the sediment water interface. Samples containing minor phosphatized carbonate microfossils and coprolites accompanied by abundant silicified carbonate microfossils would indicate normally oxygenated conditions with minor phosphatization occurring in the sediments below the redox boundary during early burial and diagenesis (Butts, 2014; Gueriau et al., 2020). This combination of microfossils is the case for most samples in this study from facies SPF and SLMW in the Mount Hyatt Member (Table 2, Fig. 9) indicating that the redox boundary was below the sediment-water interface. By contrast, samples dominated by phosphatized and originally phosphatic microfossils with fewer silicified carbonate microfossils indicate a change in redox conditions to favor extensive phosphatization and phosphate preservation resulting from a shallowing of the redox boundary and pore water dysoxia (Briggs et al., 1993; Briggs and Wilby, 1996; Briggs, 2003). This may be the result of low sedimentation rates and condensation associated with flooding surfaces or the development of dysoxic conditions at the seafloor (Catuneanu, 2006; Föllmi, 2016; Dattilo et al., 2019; Freeman et al., 2019). These samples are most commonly seen in outer ramp facies PLM and in lower Mount Hyatt Member mid-ramp facies SPF (e.g., WH 2, LLDW 31.1, LLDW 42.3, LLDW 44.2) (Table 2). Samples displaying primarily original phosphate with potential dissolution features, phosphatized, and pyritized microfossils would then represent further changes in redox conditions including low oxygen and reduced pH at or near the sediment-water interface (Sawlowicz, 1993; Wignall and Newton, 1998; Schoonen, 2004). This combination is only seen in samples of facies SLMW from the uppermost Mount Hyatt Member (MC 5.9 and MC 8). In samples containing pyrite framboids (e.g., MC 5.9), conditions may have become euxinic at the seafloor (Wilkin et al., 1996; Wignall and Newton, 1998; Rickard, 2019). With this combination of facies analysis and microfossil preservation analysis, it may be possible to track oxygenation and the early onset of acidification through more of

the Gabbs Formation.

4.3.3. Taphonomic patterns and tracking shifts in redox conditions

The observed progression of microfossil preservation from common silicification, to common original phosphate and phosphatization, and finally to pyritization within the Mount Hyatt Member of the Gabbs Formation provides a potential fossil proxy for the onset of acidifying conditions prior to the end-Triassic extinction event. By considering the associations of each preservation style in a sample, both what is present and what type of microfossils are being preserved, it is possible to distinguish baseline seafloor conditions from altered redox states in the pore water and near the sediment-water interface. Phosphatized microfossils and organic material (e.g., coprolites and chitin) found in association with abundant original silica and silicified microfossils [which do not indicate significant changes in pore water oxygenation or pH (Butts, 2014)] are likely the result of authigenic mineral growth during low sedimentation that is predicted in deeper-water facies and on flooding surfaces (Catuneanu, 2006; Föllmi, 2016). This is the case for phosphatized carbonate macrofossils and coprolites from facies PLM in the Nun Mine Member and phosphatized carbonate and moldic microfossils in the lower samples of facies SPF in the lower Mount Hvatt Member (LLDW 31.1, LLDW 42.3, LLDW 44.2). Likewise, the occasional occurrence of phosphatized microfossils in many samples from the Mount Hyatt Member in the Windy Hill, Lower Luning Draw West, and New York Canyon Road measured sections (Table 2) can be attributed to the tendency of many fossiliferous macrofossil samples, the sediments from which were used in this study, to be located near the tops of beds often on flooding surfaces. Freeman et al. (2019) and Dattilo et al. (2019) proposed a similar method of condensation to explain accumulations of small phosphatic internal molds in the Ordovician carbonates of the Cincinnati Arch without exceptional geochemical circumstances. However, the microfossil assemblages from the youngest samples from the Mount Hyatt Member (MC 5.9 and MC 8), though also containing an abundance of apatite and phosphatized fossils, do not resemble the condensed samples. Samples MC 5.9 and MC 8 display fewer silicified or phosphatized carbonate and original silica microfossils (Table 2). These types of microfossils are common in older likely condensed samples with abundant phosphatic microfossils, indicating the presence and relative abundance of these organisms in the environment. The rarity of silicified and phosphatized carbonate and original silica fossils in these youngest samples may indicate a decline of these organisms not only a taphonomic bias from condensation.

The Muller Canvon sample association of primarily original phosphate (apatite) and phosphatized microfossils is indicative of altered redox conditions during burial or early diagenesis. The assemblages in MC 5.9 and MC 8, likely the youngest microfossil samples, are dominated by originally phosphate and phosphatized microfossils, as well as common phosphatized coprolites. Some fragmentary bivalve microfossils remain silicified, but other originally carbonate fossils, such as echinoderm material, are very rare and/or phosphatized. This association implies a decrease in carbonate microfossil silicification which may be a result of early dissolution in the low pH pore water necessary to produce abundant phosphatization. In addition to the prevalence of phosphatic microfossils, pyritization of originally apatite fossils is seen commonly in samples MC 5.9 and MC 8. This dominance of phosphatic microfossils is not observed in older samples from facies SLMW and suggests that changes in the pore water geochemistry influenced early diagenesis.

The further pyritization of originally phosphate (apatite) microfossils, partial dissolution of apatite and phosphatized microfossils, and the presence of pyrite framboids in sample MC 5.9 indicates a significant shift in the redox boundary and is likely an early indication of more widespread acidifying conditions (Fig. 9). Brassy pyritization of microfossil teeth from sample MC 5.9) can be seen under magnification and was confirmed by SEM EDS analysis (Fig. 6L–M, Q–R). This is often associated with the partial dissolution of both originally phosphatic

microfossils (Fig. 6L) and phosphatized microfossils (including coprolites) giving the fossils a rough texture and making detailed identification difficult. Dissolution features on apatite and phosphatized microfossils can also be seen on a micron scale in SEM images (Fig. 6). The solubility of phosphate increases significantly as pH is lowered into acidic values (Oxmann et al., 2010; Oxmann and Schwendenmann, 2014) while pyrite deposition remains unaffected. Pyrite framboids found in the replaced areas of teeth in MC 5.9, one of the youngest samples, indicates the onset of acidifying conditions not experienced by older SLMW or deeper-water samples. In addition, pyrite framboids signal that pore water conditions were extreme for the inner-shelf transition, facies SLMW, to experience without a significant flooding surface or stratigraphic boundary, which is not indicated by a change in lithology or visible surface in the measured section. Therefore, the presence of pyrite framboids may be a sign of earlier periods of acidifying and anoxic conditions during the Rhaetian.

The taphonomy of microfossils in the upper Mount Hyatt Member are better proxies for shifting geochemical conditions than changes in lithology or macrofossil assemblages. Clement and Tackett (2021) demonstrated that the disappearance of carbonate facies in the Gabbs Formation, sometimes considered an indicator of acidification in global reviews (Greene et al., 2012), is related to a gradual facies change that begins well below the documented negative CIE coinciding with the mass extinction interval (Guex et al., 2004; Thibodeau et al., 2016; Larina et al., 2021). Macrofossil assemblages also undergo a change in the upper Mount Hyatt Member (Laws, 1978, 1982), and above the NRB, as measured by Tackett et al. (2014). Above the NRB, as indicated by the SIE, fossiliferous beds become more rare, likely owing, in part, to the progressive shallowing of carbonate dominated mid-ramp environments (facies SPF) to mixed carbonate-siliciclastic inner-ramp transition environments (facies SLMW) (Clement and Tackett, 2021). A further decline in macrofossils, potentially related to redox fluctuations in the Rhaetian, is therefore difficult to detect in the more sparsely fossiliferous facies SLMW without extreme sampling effort. It is only in the differential preservation of the microfossil samples, within this established stratigraphic framework that changes in the redox conditions are detected (Fig. 9). The acidifying conditions indicated by the dissolving phosphate and pyrite framboids of sample MC 5.9 are unlikely to have persisted until the negative CIE at the end of the Rhaetian (marking the end-Triassic extinction interval, but it is evidence for early pulses of acidification through the Rhaetian similar to the precursor excursion documented by Larina et al. (2021).

4.4. Decline of stationary calcareous epifaunal taxa through the Norian-Rhaetian boundary

Previous work has addressed paleoecological changes in the macrofossil assemblage up to the NRB. Patterns of paleoecological change in the late Norian were primarily reported from shelly fauna such as brachiopods and molluscs. Tackett and Bottjer (2016) found a decline in stationary epifaunal taxa in lower Norian deposits of Italy and Nevada and a coincident increase in mobile infaunal taxa in upper Norian deposits approaching the NRB, as indicated by the strontium isotope excursion (SIE), in the Luning and Gabbs formations of Nevada. This is a similar pattern to the Tethyan realm represented in the Lombardian Alps of northern Italy, where mobile infauna eventually dominated over stationary epifauna, though the overall transition is more gradual (Tackett and Bottjer, 2012). These findings are in agreement with other lower Norian findings of predominately stationary epifauna from the Wallowa Terrane of eastern Oregon (Newton et al., 1987) and the reduction of stationary epifaunal reefs in the Rhaetian of Japan (Peybernes et al., 2016) as well as the higher extinction rates found for sessile groups than mobile taxa in the Rhaetian (Kiessling et al., 2007). Likewise, paleoecological work immediately prior to the TJB in the Gabbs Formation from Larina et al. (2021) found more diversity among mobile infaunal taxa despite high abundance of a few

stationary epifaunal taxa. These previous results imply that the low diversity and abundance of stationary epifaunal macroinvertebrates was maintained across the NRB, and that diversity remained low up to the TJB.

This study suggests that the decline of stationary epifauna is also detectable for echinoderm taxa using microfossil assemblages. Two types of echinoderm microfossils were recovered from sample residues, echinoderm stereom and spines (Fig. 2O; 6E-G). Echinoderm stereom is ubiquitous to echinoderm taxa including crinoids, echinoids, and asteroids, and may therefore represent mobile or immobile epifaunal echinoderm taxa; however, echinoderm spines are typically attributed to urchins, which are considered fully motile. Echinoderm stereom fragments were particularly abundant in facies SPF (up to 89% of the biosediment assemblages) and were also found in facies SLMW. Likewise, echinoderm spines were found in both facies SPF and SLMW, though at lower more consistent values (0-18%). Echinoderm stereom decreased through the NRB in facies SPF, and into the Rhaetian in facies SLMW, while the proportion of echinoderm spines found in samples remained relatively constant (Fig. 8). The declining abundance of echinoderm stereom and persistent proportion of echinoderm spines implies that the contribution of echinoderm stereom from mobile urchin taxa likely remained a consistent input to the biosedimentary assemblages. The decrease in non-spine echinoderm stereom is therefore unlikely due to a decrease in all echinoderms and may instead be attributed to the relative decline of stationary epifaunal echinoderms (e.g., crinoids) as other known biosedimentary producers in these environments (Clement and Tackett, 2021). While crinoid stereom is certainly present in samples of facies SPF and the hashy skeletal packstone facies (not considered in this study) based on the presence of central canal (Clement and Tackett, 2021 Fig. 3E), the vast majority of non-spine stereom fragments is not identifiable to an echinoderm family, so further interpretation of these trends would be speculative.

The present study highlights the role of microfossils in paleobiological and paleocological reconstructions. Some taxa reported herein represent microscopic taxa, such as radiolarians, foraminiferans, and ostracods, but the most abundant taxa observed were disaggregated biogenic sediments of macroscopic life, including poriferans, bivalves, gastropods, vertebrates, and echinoderms. In this way, analysis of the largest size fraction of sediments (>250 μm) allows for an enhanced understanding of the biodiversity of larger taxa in fossil samples. The future addition of smaller size fractions will doubtlessly increase the representation of microscopic taxa and help provide the most complete representation of benthic marine diversity, paleoecology, and taphonomy. The addition of microfossil assemblages produces a dual record of life in the system that has important quantitative caveats, but nevertheless increases known diversity and exhibits shifts in abundance and diversity as shaped by environmental factors.

4.5. Causal agents across the Norian-Rhaetian boundary

A combination of geochemical, paleobiological, and diagenetic shifts are observed across the NRB in the Gabbs Formation, including a negative strontium isotope excursion, a negative carbon isotope excursion, a proliferation of silica-limited taxa, and silicification of carbonate microfossils (Fig. 9). The global nature of the strontium isotope excursion (Kovács et al., 2020) and carbon isotope excursion (Rigo et al., 2020) suggest that the driving event must have been substantial. The sudden appearance of hyper-silicifying sponges in shallow marine environments across the NRB and in the lower Rhaetian deposits suggests an increased input of dissolved silica (DSi), which is not likely to be sourced from continental weathering as indicated by the synchronous negative strontium isotope excursion. Likewise, Central Atlantic magmatic province (CAMP) volcanism is unlikely to be the cause of the observed changes, as radiogenic dates of lava flows and sills postdate the NRB by several million years (Schaltegger et al., 2008; Schoene et al., 2010; Davies et al., 2017). Other workers have suggested that the strontium isotope excursion observed across the NRB could be attributed instead to the weathering of unradiogenic carbonates or the formation of tectonic basins hindering the flow of radiogenic continental material into the oceans (Kovács et al., 2020). Neither of these alternative scenarios alone account for the coincident increase in DSi indicated in this study, nor the negative CIE and marine extinctions noted by Rigo et al., 2020; however, hydrothermal vent degassing can source both isotopically light strontium and dissolved silica (Korte et al., 2003).

The proliferation of hypersilicified sponges, the long residence time of strontium (>1 million years), the global CIE, and significant marine extinctions (Rigo et al., 2020) suggest that an increase in hydrothermal venting would be a necessary component to this suite of sedimentary features. Of the multiple hypotheses for the NRB extinctions, enhanced hydrothermal vent activity would explain the suite of characters observed in the Gabbs Formation, however this feature would also be expected to be observed in multiple localities, requiring further biosedimentary research in addition to standard isotopic measurements.

5. Conclusions

Microfossil assemblages from carbonate deposits in the Gabbs Formation exhibited paleoenvironmental affinities that shifted within and above the strontium isotope excursion (SIE), consistent with increased hydrothermal or volcanic input to marine waters close to the Norian–Rhaetian boundary (NRB). Silica-limited sponge taxa became more abundant in the SIE stratigraphic interval, and common echinoderm stereom fragments became rarer. This combination of faunal, sedimentological, and geochemical features is consistent with deteriorating conditions in the region in the latest Norian and persistent throughout much of the Rhaetian Stage.

Microfossils across the NRB and into the middle Rhaetian in New York Canyon reflect a geochemical cascade that affected the living community and subsequent diagenesis of its constituent biominerals. Spicules from lithistid demosponges and hexactinellid sponges support an abundance of water column dissolved silica (DSi), which destabilized in the near subsurface and silicified many originally carbonate grains. Increasingly acidic and anoxic pore water conditions are indicated by phosphatized microfossils and phosphatic microfossils with pyrite replacement. Together these diagenetic features indicate a slowly degrading shallow marine environment throughout much of the Rhaetian interval, culminating in the end-Triassic mass extinction.

While the causes for the global faunal turnover across the NRB are not entirely clear, the combination of abundant silica-limited marine organisms in shallow marine systems, a negative SIE, and a negative CIE provides a unique event fingerprint. Increased hydrothermal venting or subaqueous basalt emplacement would provide a source of isotopically light strontium and carbon, as well as a source of dissolved silica. An early rifting phase of Central Atlantic magmatic province (CAMP) would be consistent with step-wise environmental degradation observed during the short, volatile Rhaetian Stage, and this has important implications for our understanding of environmental shifts related to intervals of increased temperature and ocean acidification like that of the latest Triassic and in the present day.

Microfossil assemblages, when tied to specific facies and stratigraphic context, can serve as geochemical proxies for a wide range of conditions and shifts. In New York Canyon, the suite of geochemically-informative microfossils suggest that the strontium isotope excursion coincided with increased dissolved silica concentrations followed by increasingly anoxic and reducing conditions approaching the end-Triassic mass extinction interval. A microfossil assemblage approach has enormous potential for paleoenvironmental reconstruction, in particular during enigmatic intervals involving some combination of warming, acidification, and redox shifts.

Supplementary data to this article can be found online at https://doi. org/10.1016/j.palaeo.2024.112034.

Table 1. Microfossil assemblages identified by taxonomic group and

taphonomic condition. Sample names indicate the locality and the stratigraphic position of the sample in meters from the measured sections in Clement and Tackett (2021) (e.g., sample NYC 35.7 is from the New York Canyon Road locality at meter 35.7). Locality names: WH-Windy Hill, MT- Mine Test, LLDW- Lower Luning Draw West, LD- Luning Draw, NYC- New York Canyon Road, MC- Muller Canyon.

CRediT authorship contribution statement

Annaka M. Clement: Conceptualization, Data curation, Formal analysis, Funding acquisition, Investigation, Methodology, Visualization, Writing – original draft. Lydia S. Tackett: Conceptualization, Funding acquisition, Investigation, Methodology, Project administration, Resources, Supervision, Writing – review & editing. Samuel Marolt: Investigation.

Declaration of competing interest

The authors declare the following financial interests/personal relationships which may be considered as potential competing interests:

Lydia S. Tackett reports financial support was provided by National Science Foundation. Annaka M. Clement reports financial support was provided by Geological Society of America. Annaka M. Clement reports financial support was provided by Association of Applied Paleontological Sciences.

Data availability

I have shared the link to my data at the Attach File stage

Acknowledgements

This research was conducted on the traditional lands of the Northern Paiute and their ancestors. American settlers and the Government of the United States forcibly removed the Northern Paiute people from much of their homeland, including the area of this research, in the mid 1800's. Their descendants are part of the Walker River Paiute Tribe and many reside on the Walker River Paiute Indian Reservation.

This research was supported by the National Science Foundation (NSF)[CAREER Award #1654088] to Lydia Tackett, the NDSU Schwert Endowment, the Geological Society of America [Graduate Student Research Grant], and the Association of Applied Paleontological Sciences [James R. Welch Scholarship] to Annaka Clement. This material is based upon work supported by the National Science Foundation under Grant No. 0619098. Any opinions, findings, and conclusions or recommendations expressed in this material are those of the author(s) and do not necessarily reflect the views of the National Science Foundation.

The authors would like to thank North Dakota State University Department of Earth, Environmental, and Geospatial Sciences and NDSU students Joel Schock, Haley Marston, Sara Gibbs-Schnucker, Emily Nelson, Deron Zierer, Bailee McEvers, Catherine Bunker, and Emily Jackson for microfossil work.

References

- Agassiz, J.L.R., 1843. Recherches sur les poissons fossiles. Tome 3, concernant l'histoire de l'ordre des placoïdes. Imprimerie Petitpierre, Neuchâtel, 390 \pm 34 pp.
- Alvarez, B., Frings, P.J., Clymans, W., Fontorbe, G., Conley, D.J., 2017. Assessing the potential of sponges (Porifera) as indicators of ocean dissolved Si concentrations. Front. Mar. Sci. 4, 1–13. https://doi.org/10.3389/fmars.2017.00373.
- Bachan, A., Payne, J.L., 2016. Modelling the impact of pulsed CAMP volcanism on pCO2 and δ13C across the Triassic–Jurassic transition. Geol. Mag. 153, 252–270. https://doi.org/10.1017/S0016756815000126.
- Brett, C.E., Baird, G.C., 1986. Comparative taphonomy: a key to paleoenvironmental interpretation based on fossil preservation. Palaios 1, 207–227.
- Briggs, D.E.G., 2003. The role of decay and mineralization in the preservation of soft-bodied fossils. Annu. Rev. Earth Planet. Sci. 31, 275–301. https://doi.org/10.1146/annurev.earth.31.100901.144746.

- Briggs, D.E.G., Wilby, P.R., 1996. The role of the calcium carbonate-calcium phosphate switch in the mineralization of soft-bodied fossils. J. Geol. Soc. Lond. 153, 665–668. https://doi.org/10.1144/gsjgs.153.5.0665.
- Briggs, D.E.G., Kear, A.J., Martill, D.M., Wilby, P.R., 1993. Phosphatization of soft-tissue in experiments and fossils. J. Geol. Soc. Lond. 150, 1035–1038.
- Butts, S.H., 2014. Silicification. The Paleontological Society Papers 20, pp. 15–34. https://doi.org/10.1017/S1089332600002783.
- Butts, S.H., Briggs, D.E.G., 2011. Silicification through time. In: Allison, P.A., Bottjer, D. J. (Eds.), Taphonomy: Process and Bias through Time, Topics in Geobiology, pp. 411–434. https://doi.org/10.1007/978-90-481-8643-3.
- Callegaro, S., Rigo, M., Chiaradia, M., Marzoli, A., 2012. Latest Triassic marine Sr isotopic variations, possible causes and implications. Terra Nova 24, 130–135. https://doi.org/10.1111/j.1365-3121.2011.01046.x.
- Canty, A., Ripley, B., 2021. boot: Bootstrap R (S-Plus) Functions. R package version 1.3-
- Catuneanu, O., 2006. Principles of Sequence Stratigraphy, 1st ed. Elsevier, Amsterdam, p. 375.
- Cermeño, P., Falkowski, P.G., Romero, O.E., Schaller, M.F., Vallina, S.M., 2015. Continental erosion and the Cenozoic rise of marine diatoms. Proc. Natl. Acad. Sci. 112, 4239–4244. https://doi.org/10.1073/pnas.1412883112.
- Clement, A.M., Tackett, L.S., 2021. Facies stacking and distribution in the Gabbs Formation (Late Triassic, west-Central Nevada, U.S.A.): an environmental baseline to the end-Triassic carbonate crisis. Sediment. Geol. 425, 106021. https://doi.org/ 10.1016/j.sedgeo.2021.106021.
- Clement, A.M., Tackett, L.S., Ritterbush, K.A., Ibarra, Y., 2020. Formation and stratigraphic facies distribution of early Jurassic iron oolite deposits from west Central Nevada, USA. Sediment. Geol. 395, 105537 https://doi.org/10.1016/j. sedgeo.2019.105537.
- Dattilo, B.F., Freeman, R.L., Zubovic, Y., Brett, C.E., Straw, A., Frauhiger, M., Hartstein, A., Shoemaker, L., 2019. Time-Richness and Phosphatic Microsteinkern Accumulation in the Cincinnatian (Katian) Ordovician, USA: An Example of Polycyclic Phosphogenic Condensation. https://doi.org/10.1016/j. palaeo.2019.109362.
- Davies, J.H.F.L., Marzoli, A., Bertrand, H., Youbi, N., Ernesto, M., Schaltegger, U., 2017. End-Triassic mass extinction started by intrusive CAMP activity. Nat. Commun. 8, 15596. https://doi.org/10.1038/ncomms15596.
- Davison, A.C., Hinkley, D.V., 1997. Bootstrap Methods and Their Applications. Cambridge University Press, Cambridge, p. 582 (Palaeogeography, Palaeoclimatology, Palaeoecology 535, 109362).
- Dessert, C., Dupré, B., Gaillardet, J., François, L.M., Allègre, C.J., 2003. Basalt weathering laws and the impact of basalt weathering on the global carbon cycle. Chem. Geol. 202. 257–273. https://doi.org/10.1016/j.chemgeo.2002.10.001.
- Dornbos, S.Q., 2011. Phosphatization Through the Phanerozoic. In: Allison, P.A., Bottjer, D.J. (Eds.), Taphonomy: Process and Bias through Time, Topics in Geobiology, pp. 435–456. https://doi.org/10.1007/978-90-481-8643-3_12.
- Geolilogy, pp. 435–456. https://doi.org/10.100//9/8-90-481-8643-3_12.
 Dunham, R.J., 1962. Classification of carbonate rocks according to depositional textures.
 AAPG Memoirs 1, 108–121.
- Embry, A.F., Klovan, J.E., 1971. A late Devonian reef tract on northeastern Banks Island. N.W.T. Bull. Can. Petrol. Geol. 19, 730–781.
- Emmings, J.F., Poulton, S.W., Walsh, J., Leeming, K.A., Ross, I., Peters, S.E., 2022. Pyrite mega-analysis reveals modes of anoxia through geological time. Sci. Adv. 8, eabj5687. https://doi.org/10.1126/sciadv.abj5687.
- Föllmi, K.B., 1996. The phosphorus cycle, phosphogenesis and marine phosphate-rich deposits. Earth Sci. Rev. 40, 55–124.
- Föllmi, K.B., 2016. Sedimentary condensation. Earth Sci. Rev. 152, 143–180. https://doi. org/10.1016/j.earscirev.2015.11.016.
- Freeman, R.L., Dattilo, B.F., Brett, C.E., 2019. An integrated stratinomic model for the genesis and concentration of "small shelly fossil"-style phosphatic microsteinkerns in not-so-exceptional conditions. Palaeogeogr. Palaeoclimatol. Palaeoecol. 535, 109344 https://doi.org/10.1016/j.palaeo.2019.109344.
- Gallego-Torres, D., Reolid, M., Nieto-Moreno, V., Martínez-Casado, F.J., 2015. Pyrite framboid size distribution as a record for relative variations in sedimentation rate: an example on the Toarcian Oceanic Anoxic Event in Southiberian Palaeomargin. Sediment. Geol. 330, 59–73. https://doi.org/10.1016/j.sedgeo.2015.09.013.
- Greene, S.E., Martindale, R.C., Ritterbush, K.A., Bottjer, D.J., Corsetti, F.A., Berelson, W. M., 2012. Recognizing Ocean acidification in deep time: an evaluation of the evidence for acidification across the Triassic-Jurassic boundary. Earth Sci. Rev. 113, 72–93. https://doi.org/10.1016/j.earscirev.2012.03.009.
- Griffith, D.M., Veech, J.A., Marsh, C.J., 2016. Cooccur: Probabilistic Species Co-Occurrence analysis in R. J. Stat. Softw. 69, 1–17. https://doi.org/10.18637/jss. v069.c02.
- Gueriau, P., Bernard, S., Farges, F., Mocuta, C., Dutheil, D.B., Adatte, T., Bomou, B., Godet, M., Thiaudière, D., Carbonnier, S., Bertrand, L., 2020. Oxidative conditions can lead to exceptional preservation through phosphatization. Geology 48, 1164–1168. https://doi.org/10.1130/G45924.1.
- Guex, J., Taylor, D., Rakus, M., Bucher, H., 1998. Deux nouveaux genres et quatre nouvelles espece d'ammonites (Cephalopoda) du Lias inférieur. Bull. Géol. 339, 73–85.
- Guex, J., Bartolini, A., Atudorei, V., Taylor, D., 2004. High-resolution ammonite and carbon isotope stratigraphy across the Triassic-Jurassic boundary at New York Canyon (Nevada). Earth Planet. Sci. Lett. 225, 29–41. https://doi.org/10.1016/j. epsl.2004.06.006.
- Guex, J., Bartolini, A., Taylor, D., Atudorei, V., Thelin, P., Bruchez, S., Tanner, L., Lucas, S., 2009. Comment on: "the organic carbon isotopic and paleontological record across the Triassic-Jurassic boundary at the candidate GSSP section at Ferguson Hill, Muller Canyon, Nevada, USA" by Ward et al. (2007). Palaeogeogr.

- Palaeoclimatol. Palaeoecol. 273, 200–204. https://doi.org/10.1016/j.
- Guidry, M.W., Mackenzie, F.T., 2003. Experimental study of igneous and sedimentary apatite dissolution: control of pH, distance from equilibrium, and temperature on dissolution rates. Geochim. Cosmochim. Acta 67, 2949–2963. https://doi.org/10.1016/S0016-7037(03)00265-5.
- Hallam, A., Wignall, P.B., 2000. Facies changes across the Triassic-Jurassic boundary in Nevada, USA. J. Geol. Soc. Lond. 157, 49–54. https://doi.org/10.1144/jgs.157.1.49.
- Hammer, Ø., Harper, D.A.T., Ryan, P.D., 2001. PAST: paleontological statistics software package for education and data analysis. Palaeontol. Electron. 4, 1–9.
- Hartmann, J., Jansen, N., Dürr, H.H., Harashima, A., Okubo, K., Kempe, S., 2010. Predicting riverine dissolved silica fluxes to coastal zones from a hyperactive region and analysis of their first-order controls. Int. J. Earth Sci. 99, 207–230. https://doi. org/10.1007/s00531-008-0381-5.
- Huang, Y., Chen, Z.Q., Wignall, P.B., Zhao, L., 2017. Latest Permian to Middle Triassic redox condition variations in ramp settings, South China: Pyrite framboid evidence. Bull. Geol. Soc. Am. 129, 229–243. https://doi.org/10.1130/B31458.1.
- Jeppsson, L., Anehus, R., Fredholm, D., 1999. The optimal acetate buffered acetic acid technique for extracting phosphatic fossils. J. Paleontol. 73, 964–972.
- Kidwell, S.M., 1989. Stratigraphic condensation of marine transgressive records: origin of major shell deposits in the Miocene of Maryland. J. Geol. 97, 1–24.
- Kiessling, W., Aberhan, M., Brenneis, B., Wagner, P.J., 2007. Extinction trajectories of benthic organisms across the Triassic-Jurassic boundary. Palaeogeogr. Palaeoclimatol. Palaeoecol. 244, 201–222.
- Korte, C., Ullmann, C.V., 2018. Permian strontium isotope stratigraphy. Geol. Soc. Spec. Publ. 450, 105–118. https://doi.org/10.1144/SP450.5.
- Korte, C., Kozur, H.W., Bruckschen, P., Veizer, J., 2003. Strontium isotope evolution of late Permian and Triassic seawater. Geochim. Cosmochim. Acta 67, 47–62. https:// doi.org/10.1016/S0016-7037(02)01035-9.
- Korte, C., Ruhl, M., Pálfy, J., Ullmann, C.V., Hesselbo, S.P., 2019. Chemostratigraphy across the Triassic–Jurassic boundary. In: Sial, A.N., Gaucher, C., Ramkumar, M., Pinto Ferreira, V. (Eds.), Chemostratigraphy across Major Chronological Boundaries, Geophysical Monograph, vol. 240, pp. 183–210. https://doi.org/10.1002/9781119382508.ch10.
- Kovács, Z., Demangel, I., Richoz, S., Hippler, D., Baldermann, A., Krystyn, L., 2020. New constraints on the evolution of 87Sr/86Sr of seawater during the Upper Triassic. Glob. Planet. Chang. 192, 103255 https://doi.org/10.1016/j. gloplacha.2020.103255.
- Kozur, H., Mostler, H., 1971. Probleme der Conodontenforschung in der Trias. Geol.-Paläontol. Mitteilung. Innsbruck 1, 1–19.
- Larina, E., Bottjer, D.J., Corsetti, F.A., Thibodeau, A.M., Berelson, W.M., West, A.J., Yager, J.A., 2021. Ecosystem change and carbon cycle perturbation preceded the end-Triassic mass extinction. Earth Planet. Sci. Lett. 576, 117180 https://doi.org/ 10.1016/j.epsl.2021.117180.
- Laws, R.A., 1978. Paleoecology of Late Triassic Faunas from Mineral County, Nevada and Shasta County, California. M.A. thesis. University of California, Berkeley, p. 149.
- Laws, R.A., 1982. Late Triassic depositional environments and molluscan associations from west-Central Nevada. Palaeogeogr. Palaeoclimatol. Palaeoccol. 37, 131–148.
- Lei, J.Z.X., Golding, M.L., Husson, J.M., 2022. Paleoenvironmental interpretation of the late Triassic Norian – Rhaetian boundary interval in the Whitehorse Trough (Stikine Terrane, northern Canadian Cordillera). Palaeogeogr. Palaeoclimatol. Palaeoecol. 608, 111306 https://doi.org/10.1016/j.palaeo.2022.111306.
- Leys, S.P., Mackie, G.O., Reiswig, H.M., 2007. The biology of glass sponges. Adv. Mar. Biol. 52, 3–145. https://doi.org/10.1016/S0065-2881(06)52001-2.
- Li, S., Wignall, P.B., Poulton, S.W., Hedhli, M., Grasby, S.E., 2022. Carbonate shutdown, phosphogenesis and the variable style of marine anoxia in the late Famennian (late Devonian) in western Laurentia. Palaeogeogr. Palaeoclimatol. Palaeoecol. 589, 110835 https://doi.org/10.1016/j.palaeo.2022.110835.
- Lindström, S., Callegaro, S., Davies, J., Tegner, C., van de Schootbrugge, B., Pedersen, G. K., Youbi, N., Sanei, H., Marzoli, A., 2021. Tracing volcanic emissions from the Central Atlantic Magmatic Province in the sedimentary record. Earth-Sci. Rev. 212, 103444 https://doi.org/10.1016/j.earscirev.2020.103444.
- Lucas, S.G., Tanner, L.H., 2018. The Missing Mass Extinction at the Triassic-Jurassic Boundary. In: Tanner, L. (Ed.), The Late Triassic World. Topics in Geobiology 46. Springer, Cham, pp. 721–785. https://doi.org/10.1007/978-3-319-68009-5_15.
- Maechler, M., Rousseeuw, P., Struyf, A., Hubert, M., Hornik, K., 2021. cluster: Cluster Analysis Basics and Extensions. R package version 2.1.2.
- Maldonado, M., Carmona, M.C., Uriz, M.J., Cruzado, A., 1999. Decline in Mesozoic reefbuilding sponges explained by silicon limitation. Nature 401, 785–788. https://doi. org/10.1038/44560.
- Maldonado, M., Navarro, L., Grasa, A., Gonzalez, A., Vaquerizo, I., 2011. Silicon uptake by sponges: a twist to understanding nutrient cycling on continental margins. Sci. Rep. 1, 30. https://doi.org/10.1038/srep00030.
- Maldonado, M., Aguilar, R., Bannister, R.J., James, J., Conway, K.W., Dayton, P.K., Cristina, D., Gutt, J., Kelly, M., Kenchington, E.L.R., Leys, S.P., Shirley, A., Tendal, O. S., Rapp, H.T., Klaus, R., Young, C.M., 2016. Sponge grounds as key marine habitats: A synthetic review of types, structure, functional roles, and conservation concerns. In: Rossi, S. (Ed.), Marine Animal Forests. Springer International Publishing, Switzerland, pp. 1–38. https://doi.org/10.1007/978-3-319-17001-5_24-1.
- Maldonado, M., López-Acosta, M., Sitjà, C., García-Puig, M., Galobart, C., Ercilla, G., Leynaert, A., 2019. Sponge skeletons as an important sink of silicon in the global oceans. Nat. Geosci. 12, 815–822. https://doi.org/10.1038/s41561-019-0430-7.
- Maldonado, M., López-Acosta, M., Busch, K., Slaby, B.M., Bayer, K., Beazley, L., Hentschel, U., Kenchington, E., 2021. A microbial nitrogen engine modulated by bacteriosyncytia in hexactinellid sponges: ecological implications for deep-sea

- communities. Front. Mar. Sci. 8, 638505 https://doi.org/10.3389/fmars 2021 638505
- McArthur, J.M., Howarth, R.J., Shields, G.A., 2012. Strontium isotope stratigraphy. In: Gradstein, F., Ogg, J., Schmitz, M., Ogg, G. (Eds.), The Geologic Time Scale 2012. Elsevier, Amsterdam, pp. 127–144. https://doi.org/10.1016/B978-0-444-59425-9.00007.x
- Mojsisovics, E.V., 1893. Das Gebirge um Hallstatt; Abt. 1, Die Cephalopoden der Hallstätter Kalke: Abhandlungen der geologischen Reichsanstalt, Wien, Band 6, Heft 1, 2; Band 1, Supplement Heft, p. 1–356, pls. 1–70 and 1–23 (Heft 1, p. 1–82, pls. 1–32, published in 1873; Heft 2, p. 83–174, pls. 33–70, published in 1875; Supplement Heft, p. 175–356, pls. 1–23, published in 1902), pp. 1–835 pls. 71–200, 1893
- Mosher, L.C., 1968. Triassic conodonts from Western North America and Europe and their correlation. J. Paleontol. 42, 895–946. http://www.jstor.org/stable/1302396.
- Muller, S.W.M., Ferguson, H.G., 1936. Triassic and lower Jurassic formations of West Central Nevada. Bull. Geol. Soc. Am. 47, 241–252.
- Muller, S.W.M., Ferguson, H.G., 1939. Mesozoic stratigraphy of the Hawthorne and Tonopah Quadrangles, Nevada. Bull. Geol. Soc. Am. 50, 1573–1624.
- Newton, C., Whalen, M., Thompson, J., Prins, N., Delalla, D., 1987. Systematics and paleoecology of Norian (late Triassic) bivalves from a tropical island arc: Wallowa Terrane, Oregon. Paleontol. Soc. Mem. 22, 1–83.
- Oksanen, J., Simpson, G., Blanchet, F., Kindt, R., Legendre, P., Minchin, P., O'Hara, R., Solymos, P., Stevens, M., Szoecs, E., Wagner, H., Barbour, M., Bedward, M., Bolker, B., Borcard, D., Carvalho, G., Chirico, M., De Caceres, M., Durand, S., Evangelista, H., FitzJohn, R., Friendly, M., Furneaux, B., Hannigan, G., Hill, M., Lahti, L., McGlinn, D., Ouellette, M., Ribeiro Cunha, E., Smith, T., Stier, A., Ter Braak, C., Weedon, J., 2022. _vegan: Community Ecology Package_. Rpackage version 2.6–2. https://CRAN.R-project.org/package=vegan>.
- Orbigny, A.D.D', 1826. Tableau méthodique de la classe des Céphalopodes. Ann. Sci. Nat. 7 (96–169), 245–314.
- Orchard, M.J., Carter, E.S., Lucas, S.G., Taylor, D.G., 2007. Rhaetian (Upper Triassic) conodonts and radiolarians from New York Canyon, Nevada, USA. Albertiana 35, 59–65
- Oxmann, J.F., Schwendenmann, L., 2014. Quantification of octacalcium phosphate, authigenic apatite and detrital apatite in coastal sediments using differential dissolution and standard addition. Ocean Sci. 10, 571–585. https://doi.org/10.5194/os-10-571-2014.
- Oxmann, J.F., Pham, Q.H., Schwendenmann, L., Stellman, J.M., Lara, R.J., 2010.

 Mangrove reforestation in Vietnam: the effect of sediment physicochemical properties on nutrient cycling. Plant Soil 326, 225–241. https://doi.org/10.1007/s11104-009-0003-4.
- Pálfy, J., Kocsis, Á.T., 2014. Volcanism of the Central Atlantic magmatic province as the trigger of environmental and biotic changes around the Triassic-Jurassic boundary. Spec. Paper Geol. Soc. Am. 505, 245–261. https://doi.org/10.1130/2014.2505(12).
- Peybernes, C., Chablais, J., Onoue, T., Escarguel, G., Martini, R., 2016. Paleoecology, biogeography, and evolution of reef ecosystems in the Panthalassa Ocean during the late Triassic: insights from reef limestone of the Sambosan Accretionary complex, Shikoku, Japan. Palaeogeogr. Palaeoclimatol. Palaeoecol. 457, 31–51. https://doi.org/10.1016/j.palaeo.2016.05.032.
- Quéguiner, B., 2016. The Biogeochemical Cycle of Silicon in the Ocean. John Wiley & Sons Inc., Hoboken, p. 108.
- R Core Team, 2022. R: A Language and Environment for Statistical Computing. R
 Foundation for Statistical Computing, Vienna, Austria. URL. https://www.R-project.
- Read, J.F., 1985. Carbonate platform facies models. Am. Assoc. Pet. Geol. Bull. 69, 1–21. https://doi.org/10.1306/ad461b79-16f7-11d7-8645000102c1865d.
- Reuss, A.E., 1862. Entwurf einer systematischen Zusammenstellung der Foraminiferen. Sitzungsberichte der Kaiserlichen Akademie der Wissenschaften. Mathematisch-Naturwissenschaftliche Classe. Abt. 1. Mineral. Botan. Zool. Anatom. Geol. Paläontol. 44, 355–396.
- Rickard, D., 2019. How long does it take a pyrite framboid to form? Earth Planet. Sci. Lett. 513, 64–68. https://doi.org/10.1016/j.epsl.2019.02.019.
- Rigo, M., Onoue, T., Tanner, L.H., Lucas, S.G., Godfrey, L., Katz, M.E., Zaffani, M., Grice, K., Cesar, J., Yamashita, D., Maron, M., Tackett, L.S., Campbell, H., Tateo, F., Concheri, G., Agnini, C., Chiari, M., Bertinelli, A., 2020. The late Triassic Extinction at the Norian/Rhaetian boundary: biotic evidence and geochemical signature. Earth Sci. Rev. 204, 103180 https://doi.org/10.1016/j.earscirev.2020.103180.
- Ritterbush, K.A., Bottjer, D.J., Corsetti, F.A., Rosas, S., 2014. New evidence on the role of siliceous sponges in ecology and sedimentary facies development in eastern Panthalassa following the Triassic–Jurassic mass extinction. Palaios 29, 652–668.
- Ritterbush, K.A., Ibarra, Y., Tackett, L.S., 2016. Post-extinction biofacies of the first carbonate ramp of the early Jurassic (Sinemurian) in NE Panthalassa (New York Canyon, Nevada, USA). Palaios 31, 141–160. https://doi.org/10.2110/ pala/2015.021
- RStudio Team, 2022. RStudio: Integrated Development Environment for R. RStudio, PBC, Boston, MA. URL. http://www.rstudio.com/.
- Sawlowicz, Z., 1993. Pyrite framboids and their development: a new conceptual mechanism. Geol. Rundsch. 82, 148–156. https://doi.org/10.1007/BF00563277.
- Schaller, M.F., Wright, J.D., Kent, D.V., Olsen, P.E., 2012. Rapid emplacement of the Central Atlantic Magmatic Province as a net sink for CO₂. Earth Planet. Sci. Lett. 323–324, 27–39. https://doi.org/10.1016/j.epsl.2011.12.028.
- Schaltegger, U., Guex, J., Bartolini, A., Schoene, B., Ovtcharova, M., 2008. Precise U-Pb age constraints for end-Triassic mass extinction, its correlation to volcanism and Hettangian post-extinction recovery. Earth Planet. Sci. Lett. 267, 266–275. https://doi.org/10.1016/j.epsl.2007.11.031.

- Schoene, B., Guex, J., Bartolini, A., Schaltegger, U., Blackburn, T.J., 2010. Correlating the end-Triassic mass extinction and flood basalt volcanism at the 100 ka level. Geology 38, 387–390. https://doi.org/10.1130/G30683.1.
- Schoepfer, S.D., Shen, J., Sano, H., Algeo, T.J., 2022. Onset of environmental disturbances in the Panthalassic Ocean over one million years prior to the Triassic-Jurassic boundary mass extinction. Earth Sci. Rev. 224, 103870 https://doi.org/ 10.1016/j.earscirev.2021.103870.
- Schoonen, M.A.A., 2004. Mechanisms of sedimentary pyrite formation. Geol. Soc. Am. Spec. Pap. 379, 117–134.
- Shawar, L., Halevy, I., Said-Ahmad, W., Feinstein, S., Boyko, V., Kamyshny, A., Amrani, A., 2018. Dynamics of pyrite formation and organic matter sulfurization in organic-rich carbonate sediments. Geochim. Cosmochim. Acta 241, 219–239. https://doi.org/10.1016/j.gca.2018.08.048.
- Tackett, L.S., Bottjer, D.J., 2012. Faunal Succession of Norian (Late Triassic) level-bottom benthos in the Lombardian Basin: implications for the timing, rate, and nature of the early Mesozoic marine revolution. Palaios 27, 585–593. https://doi.org/10.2110/ palo.2012.p12-028r.
- Tackett, L.S., Bottjer, D.J., 2016. Paleoecological succession of Norian (late Triassic) benthic fauna in eastern Panthalassa (Luning and Gabbs formations, west-Central Nevada). Palaios 31, 190–202. https://doi.org/10.2110/palo.2015.070.
- Tackett, L.S., Kaufman, A.J., Corsetti, F.A., Bottjer, D.J., 2014. Strontium isotope stratigraphy of the Gabbs Formation (Nevada): implications for global Norian-Rhaetian correlations and faunal turnover. Lethaia 47, 500–511. https://doi.org/ 10.1111/jet.12075.
- Taylor, A.S., Lasaga, A.C., 1999. The role of basalt weathering in the Sr isotope budget of the oceans. Chem. Geol. 161, 199–214. https://doi.org/10.1016/S0009-2541(99) 00087-X.
- Taylor, D., Guex, J., 2002. The Triassic/Jurassic System boundary in the John Day Inlier, east-Central Oregon. Or. Geol. 64, 3–28.
- Taylor, D., Guex, J., Lucas, S.G., 2021. Ammonoids of the latest Triassic Gabbs Formation at New York Canyon, Mineral County, Nevada. Fossil Record 7, 393–425.
- Taylor, D.G., Smith, P.L., Laws, R.A., Guex, J., 1983. The stratigraphy and biofacies trends of the lower Mesozoic Gabbs and Sunrise formations, west-Central Nevada. Can. J. Earth Sci. 20, 1598–1608.
- Thibodeau, A.M., Ritterbush, K., Yager, J.A., West, A.J., Ibarra, Y., Bottjer, D.J., Berelson, W.M., Bergquist, B.A., Corsetti, F.A., 2016. Mercury anomalies and the timing of biotic recovery following the end-Triassic mass extinction. Nat. Commun. 7, 11147. https://doi.org/10.1038/ncomms11147.

- Tréguer, P., Nelson, D.M., van Bennekom, A.J., Demaster, D.J., Leynaert, A., Quéguiner, B., 1995. The silica balance in the world ocean: a reestimate. Science 268, 375–379. https://doi.org/10.1126/science.268.5209.375.
- Tréguer, P.J., Sutton, J.N., Brzezinski, M., Charette, M.A., Devries, T., Dutkiewicz, S., Ehlert, C., Hawkings, J., Leynaert, A., Liu, S.M., Llopis Monferrer, N., López-Acosta, M., Maldonado, M., Rahman, S., Ran, L., Rouxel, O., 2021. Reviews and syntheses: the biogeochemical cycle of silicon in the modern ocean. Biogeosciences 18, 1269–1289. https://doi.org/10.5194/bg-18-1269-2021.
- Uriz, M.J., Turon, X., Becerro, M.A., Agell, G., 2003. Siliceous spicules and skeleton frameworks in sponges: origin, diversity, ultrastructural patterns, and biological functions. Microsc. Res. Tech. 62, 279–299. https://doi.org/10.1002/jemt.10395
- Van Cappellen, P., Dixit, S., van Beusekom, J., 2002. Biogenic silica dissolution in the oceans: reconciling experimental and field-based dissolution rates. Glob. Biogeochem. Cycles 16. https://doi.org/10.1029/2001gb001431, 23-1-23-10.
- Veizer, J., Ala, D., Azmy, K., Bruckschen, P., Buhl, D., Bruhn, F., Garden, G.A.F., Diener, A., Ebneth, S., Godderis, Y., Jasper, T., Korte, C., Pawellek, F., Podlaha, O.G., Strauss, H., 1999. ⁸⁷Sr, ⁸⁶Sr, δ¹³C and δ¹⁸O evolution of Phanerozoic seawater. Chem. Geol. 161, 59–88. https://doi.org/10.1016/S0009-2541(99)00081-9.
- Ward, P.D., Garrison, G.H., Williford, K.H., Kring, D.A., Goodwin, D., Beattie, M.J., McRoberts, C.A., 2007. The organic carbon isotopic and paleontological record across the Triassic-Jurassic boundary at the candidate GSSP section at Ferguson Hill, Muller Canyon, Nevada, USA. Palaeogeogr. Palaeoclimatol. Palaeoecol. 244, 281–289. https://doi.org/10.1016/j.palaeo.2006.06.042.
- Wignall, P.B., Newton, R., 1998. Pyrite framboid diameter as a measure of oxygen defiiency in ancient mudrocks. Am. J. Sci. 298 https://doi.org/10.2475/ajs.298.7.537, 573–552.
- Wignall, P.B., Newton, R., Brookfield, M.E., 2005. Pyrite framboid evidence for oxygen-poor deposition during the Permian-Triassic crisis in Kashmir. Palaeogeogr. Palaeoclimatol. Palaeoecol. 216, 183–188. https://doi.org/10.1016/j.palaeo.2004.10.009.
- Wilkin, R.T., Barnes, H.L., Brantley, S.L., 1996. The size distribution of framboidal pyrite in modern sediments: an indicator of redox conditions. Geochim. Cosmochim. Acta 60. 3897–3912.
- Zaffani, M., Agnini, C., Concheri, G., Godfrey, L., Katz, M., Maron, M., Rigo, M., 2017. The Norian "chaotic carbon interval": new clues from the δ¹³C_{org} record of the Lagonegro Basin (southern Italy). Geosphere 13, 1–16. https://doi.org/10.1130/ GFS01459.1.
- Zaffani, M., Jadoul, F., Rigo, M., 2018. A new Rhaetian δ13Corg record: Carbon cycle disturbances, volcanism, End-Triassic mass Extinction (ETE). Earth Sci. Rev. 178, 92–104. https://doi.org/10.1016/j.earscirev.2018.01.004.